Reactivity and bioconcentration of stable cesium in a hyperturbid fluvial-estuarine continuum: A combination of field observations and geochemical modeling

Teba Gil-Díaz, Frédérique Pougnet, Maëva Labassa, Lionel Dutruch, Melina Abdou, Alexandra Coynel, Frederique Eyrolle, Nicolas Briant, Joël Knoery, Jörg Schäfer

HAL Id: insu-04572992

https://insu.hal.science/insu-04572992

Submitted on 16 May 2024

Reactivity and bioconcentration of stable cesium in a hyperturbid fluvial-estuarine continuum: A combination of field observations and geochemical modeling

Teba Gil-Díaz [a,b,*], Frédérique Pougnet [a], Maëva Labassa [a], Lionel Dutruch [a,c], Melina Abdou [a], Alexandra Coynel [a], Frédérique Eyrolle [d], Nicolas Briant [e], Joël Knoery [e], Jörg Schäfer [a]

[a] Univ. Bordeaux, CNRS, Bordeaux INP, EPOC, UMR 5805, F-33600 Pessac, France
[b] Institute of Applied Geosciences, Karlsruhe Institute of Technology, Adenauerring 20b, 76131 Karlsruhe, Germany
[c] Université de Rennes, UMR CNRS 6118, Campus Beaulieu 35000 Rennes, France
[d] Institut de Radioprotection et de Sureté Nucléaire (IRSN), PSE-ENV, STAAR/LRTA, BP 3, 13115 Saint-Paul-lez-Durance, France
[e] Ifremer, CCEM Contamination Chimique des Écosystèmes Marins, F-44000 Nantes, France

HIGHLIGHTS

- Unique comprehensive work on stable Cs in continent-ocean transition system.
- Watershed reactivity depends on geological source and seasonal processes.
- Non-conservative estuarine behavior, driven by SPM age and salinity.
- Modeled conditions show main sorption driver is cation-exchange with clay fraction.
- Low BCFs in oysters but general natural origin of Cs related to water discharge.

GRAPHICAL ABSTRACT
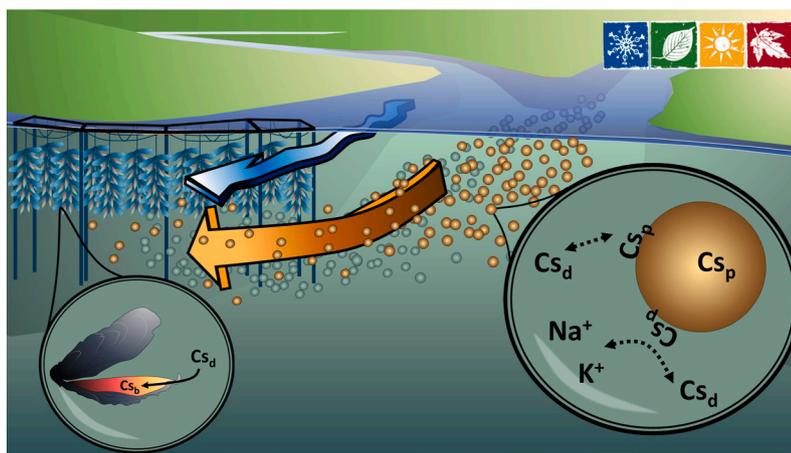
ARTICLE INFO

Handling Editor: Milena Horvat

ABSTRACT

Effective, post-accidental management needs an accurate understanding of the biogeochemical behavior of radionuclides in surface environments at a regional scale. Studies on stable isotopes (element homologs) can improve this knowledge. This work focuses on the biogeochemical behavior of stable cesium (Cs) along a major European fluvial-estuarine system, the Gironde Estuary (SW France). We present results obtained from (i) a long-term monitoring (2014–2017) of dissolved (Cs_d) and particulate (Cs_p) Cs concentrations at five sites along the freshwater continuum of the Garonne watershed, (ii) Cs_d and Cs_p concentrations during four oceanographic campaigns at contrasting hydrological conditions along longitudinal profiles of the estuarine system, (iii) a 24 h

* Corresponding author. Institute of Applied Geosciences, Karlsruhe Institute of Technology, Adenauerring 20b, 76131 Karlsruhe, Germany.
  E-mail address: teba.gil-diaz@kit.edu (T. Gil-Díaz).

Clay minerals
PhreeqC

cycle of Cs_p at the estuary mouth, and (iv) a historical trend of Cs bioconcentration in wild oysters at the estuary mouth (RNO/ROCCH, 1984–2017). In addition, we model the partitioning of Cs within the estuarine environment for clay mineral interactions via PhreeqC. At fluvial sites, we observe a geogenic dependence of the Cs_p and a seasonal variability of Cs_d, with a downstream increase of the solid-liquid partitioning ($\log_{10}$ Kd values from 3.64 to 6.75 L kg^{-1}) for suspended particulate matter (SPM) < 200 mg L^{-1}. Along the estuarine salinity gradients, Cs shows a non-conservative behavior where fresh SPM (defined as Cs-depleted particles recently put in contact with Cs_d) act as a Cs sink during both flood and low discharge (drought) conditions. This sorption behavior was explained by the geochemical model, highlighting the relevance of ionic strength, water and SPM residence times. However, at high salinities, the overall $\log_{10}$ Kd value decreases from 6.02 to 5.20 for SPM ~300–350 mg L^{-1} due to the Cs_d oceanic endmember. Despite wild oysters showing low bioconcentration factors (~1220 L kg^{-1}) at the estuary mouth, they are sensitive organisms to Cs fluxes.

1. Introduction

Monitoring programs provide a "black-box", i.e., macroscopic/generalized view on the overall transport and reactivity of trace elements and data, crucial in supporting process studies. These programs include systematic collection of a wide variety of matrices including atmospheric deposition, water, sediments and/or sentinel species as indicators of temporal and spatial variabilities of trace elements. Independent of the nature of the examined element (stable or radioactive), monitoring programs allow to establish trace element distributions in ecosystems (e.g., Saito et al., 2015), and system understanding such as, e.g., the resilience of the environment affected by contaminated events/sites (e.g., Pougnet et al., 2022). However, when target elements fall below the levels of concern for human health, the time series are often disregarded, even though they also provide information about ecosystem dynamics and/or insights to homolog trace element behavior. Such is the case for stable cesium (Cs), for which there are only three point published works in the literature (Shim et al., 2012; Takata et al., 2013; Bera et al., 2015) and no temporal series.

In addition, few monitoring programs go beyond the data collection and plotting, trying to combine both field observations with mechanistic process-understanding, providing an explanation to the recorded long-term series of element concentrations in a given system. Process-understanding could be achieved via modeling of physical-chemical and solid-liquid interactions of trace elements. Here we refer to geochemical models and not empirical models based on field/experimental data. In fact, this approach is widely used in the field of migration of radionuclides in deep geological storage sites and for coastal dispersion of radionuclide releases from nuclear fuel reprocessing plants (e.g., Periáñez and Elliott, 2002), but not yet systematically applied for stable elements in surface aquatic systems. Furthermore, geochemical models combining solid-liquid interfacial processes (i.e., cation exchange and/or surface complexation models) with advection/diffusion transport are still scarce in the literature, particularly for surface aquatic environments and stable elements below levels of concern.

Geochemical models require several parameters (e.g., surface area, cation exchange capacity, element speciation, surface functional binding groups, thermodynamic data, etc.), which are quantified under controlled conditions. This information exists in the literature for certain elements of concern/interest but not for all the periodic table and not all substrates (e.g., example of selenium, related to the toxicity of its stable forms at high concentrations and the persistence of its radioactive forms for nuclear waste storage sites; Missana et al., 2009; Nie et al., 2017). This is also the case for radioactive Cs as, due to its radiological relevance in nuclear activities, there is relatively advanced knowledge on physical-chemical parameters (e.g., Gutierrez and Fuentes, 1996; Bradbury and Baeyens, 2000; Missana et al., 2014). Nevertheless, there is still little understanding about Cs transport and reactivity in hydro-systems at the continent-ocean interface. For instance, Sanial et al. (2017) discovered after the Fukushima Daiichi nuclear power plant accident in 2011 that underground estuaries from the coast of Japan were unexpectedly acting as long-term secondary sources of ^{137}Cs. Therefore, providing a more mechanistic understanding of Cs reactivity,

dispersion and fate in surface aquatic systems, even based on homolog stable Cs behavior, is also a requirement to improve post-accidental management of radionuclide releases at a regional scale.

This work aims at: (a) providing a complete dataset from field observations regarding concentrations, reactivity and bioconcentration of stable Cs at a fluvial-estuarine continuum, and (b) verifying the usefulness of geochemical models for surficial hydro-systems as supporting tools for understanding/analyzing field observations and identifying dominant regional processes, applied for the case of the estuarine system. The study area is the Lot-Garonne-Gironde fluvial-estuarine system (SW France), presenting (i) long-term historical series (2014–2017) of dissolved (Cs_d) and particulate (Cs_p) Cs concentrations at five river sites with a monthly frequency, (ii) Cs_d and Cs_p concentrations along estuarine longitudinal profiles during four contrasting hydrological conditions (drought or low river water discharges, flood and extreme flood), (iii) a diel (24 h) cycle of Cs_p dynamics at the estuary mouth, and (iv) a historical trend of Cs bioconcentration in wild oysters at the estuary mouth (RNO/ROCCH, 1984–2017). The geochemical model involves a 1D advective/diffusive transport model, incorporating the commonly accepted cation exchange descriptions for Cs onto clays, implemented via PhreeqC. Overall, this study provides a more comprehensive knowledge on stable Cs biogeochemical cycling, complements post-accidental management studies for the dispersion and fate of radioactive Cs in surface environments, and promotes digitalization of continent-ocean transition systems (towards the development of numerical twins).

2. Material and methods

2.1. Study area: the Lot-Garonne-Gironde fluvial-estuarine system

The Lot-Garonne-Gironde fluvial-estuarine system in the SW of France (Fig. 1) has been systematically monitored for trace elements at the regional (i.e., watershed) scale for classical elements (e.g., Cd, Zn, Cu, Pb; Pougnet et al., 2022) since the 1990's, with more recent and continuous data for other trace elements since 2003 (e.g., Cd, Ag, Sb, Gd; Lanceleur et al., 2011a; Gil-Díaz et al., 2018; Lerat-Hardy et al., 2019). This monitoring program started due to the historical metal pollution and subsequent long-lasting rehabilitation works that have taken place over the years at the watershed. The monitoring program, financed by the Adour Garonne Water Agency, focuses on five representative sites along the watershed: (1) 'Boisse Penchot' (BP) on the upstream Lot River, (2) 'Riou Mort' (RM) at the outlet of the Riou Mort River hosting the historical industrial point sources of metals, (3) 'Temple' (T), at the outlet of the Lot River watershed, (4) 'Port-Sainte-Marie' (PSM), upstream the Garonne River and (5) 'La Réole' (LR), on the Garonne River downstream of its confluence with the Lot River, with the latter constituting the upper limit of the tidal influence of the Gironde Estuary. Traditionally, the city of Bordeaux represents the kilometric point (KP) 0 km of the Gironde Estuary, increasing to 110 km at the estuary mouth. In order to navigate along the studied sites and the present work, we have assigned to the acronym of each sampling site an additional code representing the associated river (i.e., Gar for Garonne River, Lot for the

Lot River, and Rio for the Riou Mort River) and the corresponding distance to Bordeaux. Positive km corresponds to downstream sites whereas negative km is assigned to sites upstream of Bordeaux (Fig. 1). The present work uses the monthly sampling campaigns between 2014 and 2017, collecting manually water and SPM samples: n = 64 at LR, n = 62 at PSM, n = 62 at T, n = 63 at BP, n = 62 at RM.

The Gironde Estuary is one of the largest estuaries in Europe and an important continent-ocean interface system towards the Atlantic Coast (Fig. 1). Its watershed has a total area of ~81 000 km^2 and receives an average freshwater discharge (Q) of ~960 m^3 s^{-1} (DIREN, 2023) mainly from the Garonne and the Dordogne rivers (Salomon, 2002; Schäfer et al., 2002). Within the estuary, water residence times vary from 86 days in low discharge conditions to ~18 days during high discharges (Castaing and Jouanneau, 1979; Jouanneau and Latouche, 1981). Contrastingly, the average residence time of suspended particulate matter (SPM) is of 1–2 years. The estuary has a strong maximum turbidity zone (MTZ of ~1000 mg L^{-1}; Castaing and Jouanneau, 1979; Sottolichio and Castaing, 1999), which is only expulsed onto the continental shelf at the co-occurrence of continuous high river discharge that displaces it towards the estuarine mouth, and spring ebb tides that push it beyond the coastline (Allen et al., 1980; Castaing and Allen, 1981; Doxaran et al., 2009). In our case, the estuarine salinity and turbidity gradients were monitored during four oceanographic campaigns, from Bordeaux to the estuary mouth on board the *R/V Thalia* (IFREMER), during contrasting hydrological conditions: MGTS I in March 2014 (n = 26; Q$_{MGTS I}$ ~1203 m^3 s^{-1}), MGTS II in March 2015 (n = 23; Q$_{MGTS II}$ ~3450 m^3 s^{-1}), MGTS III in October 2015 (n = 26; Q$_{MGTS III}$ ~206 m^3 s^{-1}) and MGTS IV in June 2017 (n = 20; Q$_{MGTS IV}$ ~235 m^3 s^{-1}). During the latter cruise, a diel cycle (24 h) collection of samples at the estuary mouth (Fig. 1) was also pursued. Further details about these campaigns and other trace elements can be found in the literature (Gil-Díaz et al. 2016, 2019; Abdou and Tercier-Waeber, 2022; Pougnet et al., 2022).

The Gironde Estuary mouth also hosts wild oysters which are regularly sampled as part of the National Network for the Observation of Marine Environment Quality (i.e., the French Mussel-Watch program; RNO/ROCCH, since 1974). This program has sampled, analyzed and stored total soft tissues of wild, two-year old (~8 cm long) Japanese oysters (*Crassostrea gigas,* cf. *Magallana gigas*) during winter (February–March) at La Fosse (Fig. 1) since 1979. This work shows only the time series of Cs from archived samples between 1984 and 2017 at a 2-year interval (n = 18). Complementary results about other trace elements can be found in the literature (Gil-Díaz et al., 2019; Pougnet et al., 2021). In addition, five samples were collected in April 2014 for organotropism scoping (i.e., gills, muscle, mantle and digestive gland), presented here as supplementary information.

2.2. Sample collection and sample treatment

2.2.1. Water and SPM for trace element quantification

In general, sub-surface water was collected either with a telescopic pole (~0.3 m depth, 1 m away from the river bank) or with a Niskin bottle (on-board at 1 m depth), into previously acid-washed polypropylene (PP) bottles. Samples were filtered on-site through 0.2 μm Minisart® cellulose acetate filters, acidified with HNO$_3$ (1/1000 v/v; J. T. Baker ultrapure, 14 M) and stored at 4 °C in the dark. At the same time, SPM samples were collected into 40 L acid washed polyethylene (PE) drums and particles were retrieved by flow-through centrifugation (Westfalia, 12 000×g; Lapaquellerie et al., 1996), followed by oven drying (50 °C), grinding and homogenized, and then, stored at room temperature in the dark until digestion.

As described in many other works (Schäfer et al., 2002; Gil-Díaz et al., 2018; Gil-Díaz et al., 2019, etc.), the representative aliquots of SPM (i.e., ~30 mg) were digested as follows. Acid-cleaned, closed PP tubes (DigiTUBEs®, SCP SCIENCE) were used with a Teflon®-coated heating block (2 h at 110 °C; SCP Science). The SPM were digested in a tri-acid mixture including 1.5 mL HCl (10 M Suprapur®, Merck), 750 μL HNO$_3$ (14 M Suprapur®, Merck) and 2.5 mL HF (29 M Suprapur®, Fisher), accounted as a "total digestion" method. After evaporation to dryness, the residues were re-dissolved with 250 μL HNO$_3$ (14 M) in the heating block, and the samples were completed to 10 mL using Milli-Q water.

2.2.2. Biological material (wild oysters)

The RNO/ROCCH program (IFREMER) collects oyster samples at La Fosse according to the guidelines for monitoring contaminants in biota (OSPAR commission; OSPAR, 2018). After depuration with particle-free water obtained from the site, whole soft bodies, pooled (20–60
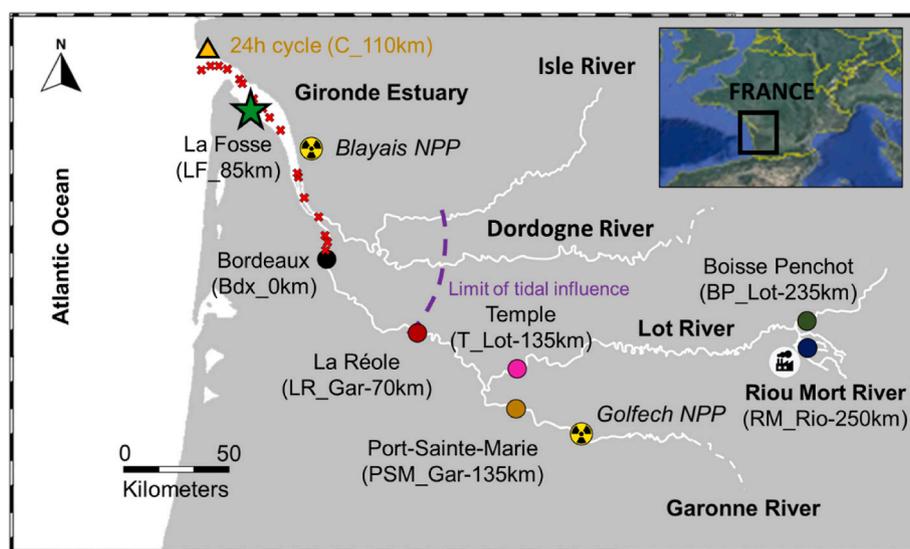
Fig. 1. Map of the Lot-Garonne-Gironde fluvial-estuarine system in the SW France. Sampling points were: (i) five freshwater sampling sites sampled between 2014 and 2017 (circles), (ii) four oceanographic campaigns performing longitudinal profiles integrating estuarine salinity and turbidity gradients (crosses), (iii) a diel cycle at the estuary mouth during drought/low water conditions (triangle), (iv) punctual coastal points, and (v) wild oysters collected between 1984 and 2017 at La Fosse (star). Current operating nuclear power plants (NPP) in the area are also included. The codes of each sampling site refer to the acronym of the site, the river where it is located, and the distance to the 0 km (Bordeaux), positive for downstream and negative for upstream sites.

individuals, depending on the size), ground, freeze-dried, and homogenized, then stored in the National Mussel Watch sample bank pending specific (element-dependent) digestions and analyses. In this work, aliquots of ~200 mg were digested in a microwave oven (ETHOS UP, Milestone Srl) with 4 mL HCl (34–37 % Suprapur®, SCP Science) and 2.8 mL HNO$_3$ (67–69 % Suprapur®, SCP Science). The temperature program was set with a ramp of $9\,°C\,min^{-1}$ up to 180 °C, then followed a 30 min digestion at 180 °C before cooling down. According to known protocols (Daskalakis et al., 1997; USEPA, 2007) and to avoid potential polyatomic interferences with Cl$^-$, these acid digestions were evaporated at 50–60 °C and recovered in HNO$_3$ matrix. A parallel study based on several bivalve samples and different masses of soft tissue supports the existence of a critical mass for obtaining reliable values of ultra-trace elements. This issue is potentially related to interferences at lower element signals as discussed for the case of Pt (Abdou et al., 2018). For Cs$_b$, this critical mass should be > 200 mg (i.e., Fig. S1).

2.2.3. Water discharge, SPM concentrations, and physical-chemical parameters

Information about the daily water discharge at each watershed studied site is available online via the National Hydrographic Databank (DIREN, 2023). Complementary SPM concentrations over time were obtained by *in situ* filtration of volumes of water through dry pre-weighed filters (Xilab glass microfiber, 0.7 μm). These filters were then dried to constant weight at 50 °C and re-weighed. Physical-chemical parameters, including water temperature and conductivity (Tetra-Con 96® probe, PROFILINE, WTW), as well as pH (Sentix® 41 probe, PROFILINE, WTW) were also measured *in situ*. These results can be found in Gil-Díaz et al., (2019).

2.3. Quantification of dissolved (Cs$_d$), particulate (Cs$_p$) and biological (Cs$_b$) cesium

Freshwater dissolved (Cs$_d$), particulate (Cs$_p$), and biological (Cs$_b$) Cs concentrations were analyzed by triple quadrupole inductively coupled plasma mass spectrometry (ICP-MS; iCAP-TQ, THERMO®) in kinetic energy discrimination (KED)-mode (He), with external calibration. No corrections for interferences were required. Detection limits (LOD) were 0.04 ± 0.01 ng L^{-1} for several analyses of 10 blanks at 2 % HNO$_3$ (J.T. Baker ultrapure). Digestion blanks (n = 3 per digestion batch) were also used to control any contamination from the digestion process (~1 ng L^{-1} for LOD of 0.06 ± 0.02 ng L^{-1}, n = 10 blanks). Brackish waters (i.e., estuarine Cs$_d$) were also analyzed directly, in this case via standard additions and gas dilution, with the ICP-MS iCAP-TQ. In these conditions, slightly higher LOD 1.20 ± 0.16 ng L^{-1} were obtained. This method is faster and equally reliable compared to other reported approaches with the same LODs but involving pre-concentration methods (e.g., ammonium 12-molybdophosphate complexation and ion exchange resin column; Takata et al., 2013).

Appropriate certified reference materials (CRM) for Cs are only available for the particulate phase. Corresponding recoveries were 85 ± 10 % (n = 30) for stream sediment NCS DC 73307, and 91 ± 16 % (n = 30) for marine sediment NIST® RM 8704. Additionally, particulate thorium (Th$_p$) was also measured in the SPM for grain-size correction purposes. Recoveries for Th were of 90 % in marine sediment NIST SRM 2702 (n = 12) and 85 % for NIST® RM 8704 (n = 36), as reported in Gil-Díaz et al., (2019). Since no CRM exists for Cs in biological materials, its reproducibility was monitored using the CRM NIST Oyster Tissue 1566b (e.g., generally used for complementary elements like Sb, Sn and Se), showing ~5 % relative standard deviations (RSDs) in microwave assisted digestions (10.1 ± 1.14 mg kg^{-1}, n = 11).

2.4. Data treatment

2.4.1. Grain size normalization

It is a common practice in geochemistry to normalize trace element

particulate concentrations. That is, certain trace elements naturally show higher concentrations in smaller particles due to the high surface area of exchange, i.e., more available adsorption sites present in the small particles compared to bigger particles (Loring and Rantala, 1992). This effect is identified by normalizing particulate concentrations against other conservative elements, which have no anthropogenic influence and show size effect behavior (Reimann and de Caritat, 2000). In our case, thorium (Th) is a conservative lithogenic trace element adequate for correcting grain size effects, particularly in silicate-dominated sediments (Krachler and Shotyk, 2004; Larrose et al., 2010). Therefore, many of the particulate results presented in this work will show both Cs concentrations in the particulate phase (Cs$_p$) as well as Th-normalized concentrations (Cs$_p$/Th$_p$), given the potential bias of particle size in Cs$_p$ quantification. Grain size effects are identified by comparing both Cs$_p$ and Cs$_p$/Th$_p$ trends, e.g., there is an influence of the grain size when two sites/sampled points show significant differences at the level of Cs$_p$ trends and not anymore when comparing Cs$_p$/Th$_p$ values.

2.4.2. Distribution coefficients (Kd)

Cesium partitioning between the dissolved and particulate phases can be described by the solid-liquid distribution coefficient (Kd; McKinley and Alexander, 1992; Sung, 1995). Briefly, Kd (in L kg^{-1}) is the ratio between Cs$_p$ (mg kg^{-1}) and Cs$_d$ (mg L^{-1}). Noteworthy, Kd presented in this work corresponds to geogenic values. This is coherent with quantitative recovery of Cs$_p$ in suspended material, not only its exchangeable forms. This Kd value is obtained from environmental concentrations, meaning that it may not always involve true equilibrium conditions. The total Cs (Cs$_T$) can be described as the sum of both Cs$_d$ and Cs$_p$. A combination of all these concepts describes the relationship between the particulate fraction of Cs$_p$ (%) and the Kd (Eq. (1); Gil-Díaz et al., 2019), according to the SPM concentration (kg L^{-1}).

$$Cs_p(\%) = 100 \cdot \frac{Cs_p \cdot SPM}{Cs_T} = 100 \cdot (Kd \cdot SPM) \Big/ (1 + Kd \cdot SPM) \qquad (1)$$

2.4.3. Annual fluxes

As described in Gil-Díaz et al., (2019), annual fluxes (kg y^{-1}) of Cs$_d$ (Eq. (2)) and Cs$_p$ (Eq. (3)) were calculated based on discharge-weighed concentrations. This approach has been commonly applied before (e.g., Meybeck et al., 1994; Meybeck and Ragu, 1995; Webb et al., 1997) and requires daily (Q$_i$) and annual (Q') average water discharges from the National Hydrographic Databank (DIREN, 2023) as well as daily SPM fluxes (F$_{SPMi}$) and Cs$_d$/Cs$_p$ concentrations from the sampling survey (~24-day frequency).

$$F_{Cs_d} = Q' \left(\sum_{i}^{n} (Q_i \cdot Cs_d) \Big/ \sum_{i}^{n} Q_i \right) \qquad (2)$$

$$F_{Cs_p} = Q' \left(\frac{\sum_{i}^{n} \left(F_{SPMi} \cdot Cs_p \right)}{\sum_{i}^{n} Q_i} \right) \text{ for } F_{SPMi} = SPM_i \cdot Q_i \qquad (3)$$

2.4.4. Bioconcentration ratios

The bioconcentration ratio provides information about the amount of trace element that has been absorbed/retained in the organism in natural conditions, including both direct (i.e., dissolved exposure) and indirect (i.e., trophic exposure) pathways. It is defined as the ratio between the trace element concentration in the organism's tissue (e.g., Cs$_b$ in mg kg^{-1}) and the concentration of trace element in the surrounding environment, at steady-state (USEPA, 2000; Arnot and Gobas, 2006). Normally, the later value corresponds to the dissolved concentration (i.e., Cs$_d$ in mg L^{-1}), since it potentially shows the highest bioavailability between dissolved and particulate forms (e.g., Lekhi et al., 2008).

2.5. Modeling Cs sorption in the Gironde Estuary

An advective and diffusive transport model was set up using the free, geochemical software PhreeqC (Parkhurst and Appelo, 1999) and the sit. dat database. The aim of this preliminary approach is to better understand the potential processes responsible for the environmental observations, building a bridge between monitoring and modeling. Nevertheless, one should bear in mind that this simulation uses uniform, average estuarine conditions, and static particles. Reality includes a geographically mobile MTZ, with expulsion events and renewal/input of fluvial particles, with a combination of tidal cycles with flood/drought long periods. Despite these potential shortcomings compared to reality, our modeling approach is still valid, as will be shown in the results section.

Known characteristics from the Gironde Estuary (Fig. 2a) were reproduced in PhreeqC with a 1D model, mimicking the estuary as a horizontal exchange column/tube (Fig. 2b). The analogy between the estuarine system (slow moving particles in a funnel with exchanging water masses from each endmember) and the packed-column system (stationary particles with water endmembers moving and mixing between the packed grains) is pertinent given the water and SPM residence times of the Gironde Estuary. In the real system, SPM and MTZ are retained for long periods of time (up to 2 years – could be seen as a stationary phase in a column) whereas water masses mix and interact on a tidal basis, and remain in the system on a daily/monthly basis (much shorter periods of time compared to SPM – could be seen as the water endmembers through the column). The size of the horizontal column is as big as the Gironde Estuary (~150 km long), with 30 cells of 5 km each, full of stationary particles. The column contains a middle area with higher particle density (i.e., packing of 1000 mg L^{-1}, simulating the MTZ) compared to the rest of the column (i.e., average packing of ~100 mg L^{-1}, simulating average estuarine SPM). This spatial evolution of the particle composition within the column is defined in PhreeqC via cell properties (e.g., cells 1–10 contain an amount of moles equivalent to the cation exchange capacity of a surface provided by 100 mg L^{-1} of particles). The particle composition follows the identified ratio between illite and smectite clay minerals for the Gironde fluvial-estuarine system (i.e., based on XRD measurements ~35 % illite and muscovite dominating clay minerals, ~10 % smectites; Gil-Díaz et al., 2020), brought to the total packing density for each area (e.g., in 100 mg L^{-1}, ~77 mg L^{-1} are illites and ~23 mg L^{-1} are smectites).

Flood and ebb conditions along the entire estuary were mimicked with two solution endmembers flowing back and forth through the column (visual scheme of applied regimes can be found in Fig. S2). The flow conditions are modeled via the "Transport" command of PhreeqC, by alternating forward and backward flow direction. These solutions simulate seawater and freshwater matrices (full composition described in Table S1) containing 300 ng L^{-1} and 10 ng L^{-1} Cs, respectively, based on the results for Cs$_d$ obtained from this work. The velocity of the freshwater and seawater influence through the column was modified and assigned accordingly to represent flood and drought conditions based on the known average flood and drought water discharges (*c.f.* section 2.1).

Overall, three models are simulated (Table 1). Overall, the concepts of "fresh" and "old" SPM will be used along the model descriptions and the manuscript several times. The definition here of fresh SPM imply particles that are originally low in Cs$_p$ concentrations (e.g., in the environment corresponding to freshly eroded particles released into the aquatic system) and have been recently put in contact with Cs$_d$. Alternatively, old SPM refer to those particles that have been exposed to several cycles of fresh- and seawater discharges. This means that the old particles have been exposed to several exchanges between Cs$_p$ and Cs$_d$, with every independent water mass and Cs$_d$ load from each endmember. This is modeled by the time component, i.e., the packed column is composed of un-exposed particles, which over time will re-equilibrate with Cs-containing solutions. This means that the surface characteristics are not modified *per se*, they are changing over time due to re-equilibration processes between the amounts of Cs in the particulate and the dissolved phases. This also implies that, when referring to "fresh" or "old" SPM based on modeled results, we refer to a behavior observed for all the SPM within the entire column. The adsorption of Cs was modeled based on published cation-exchange parameters for average illite (Bradbury and Baeyens, 2000) and smectites (Missana et al., 2014). Despite the existence an electrostatic, triple layer (TLM), surface complexation model for Cs sorption onto montmorillonite (Gutierrez and Fuentes, 1996), this approach is not included in this work, as the previous descriptions already explained the environmental observations. The cation-exchange models are described in detail in section 4.3.1 and the model parameters used in this work are included in Table S2. The outcomes of these simulations include dissolved and particulate Cs species, concentrations, and Kd values along distance and salinity gradients.
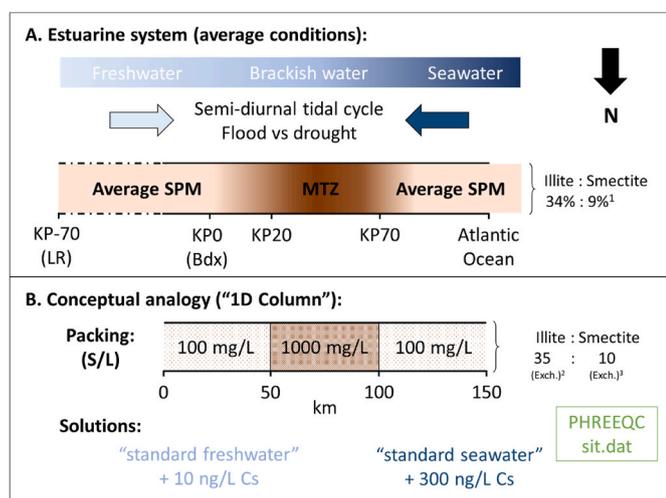

Fig. 2. Schematic parallelism between (A) the physical-chemical characteristics of the Gironde Estuary and equivalent kilometric points (KP), and (B) the conceptual 1D column used to numerically simulate the adsorption of Cs along a salinity and turbidity gradients. Abbreviations: solid to liquid ratio (S/L), cation exchange (Exch.).

Table 1
Description of the three applied models and the intended environmental analogy.

Model simulation	Approach	Environmental comparison
1	No exchange allowed between Cs$_d$ and particles, only mixture of water masses	Conservative behavior
2	Enabled cation exchange in a regime with transitional tidal flow, using intermediate flow rates for the freshwater endmember and shorter flow rates for the seawater endmember	Non-conservative behavior with fresh SPM recently introduced into the estuarine system
3	cation exchange takes place firstly during extreme flood and drought conditions (e.g., continuous flushing of the column with freshwater for flood conditions), followed by tidal flow (as in model 2).	Non-conservative behavior in old SPM held within the estuarine system

3. Results

3.1. Spatial-temporal variations of Cs

3.1.1. Four-year trends within the Garonne River watershed

The Garonne River watershed shows variable Cs concentrations (Cs_d and Cs_p) in the 4-year survey (2014–2017, Fig. 3). Highest concentrations of both Cs_d and Cs_p are found in the Lot River. The Cs_d decreases by a factor of 3 downstream of the Lot River (i.e., from BP to T, despite the 13-fold higher Cs_d from RM), and increases 2-fold within the Garonne River (i.e., from PSM to LR). In the particulate phase however, average Cs_p slightly decreases within the Lot River (i.e., factor 1.3 from BP to T, with RM showing almost half of the average Cs_p) and then decreases again by a factor of ~2 from the Lot River to the Garonne River (i.e., from T to LR). Temporally, Cs_d shows a seasonal pattern with higher concentrations in summer and lower in winter, parallel to the water discharges, particularly at RM, BP and PSM. Contrastingly, Cs_p shows sporadic influence of the grain size (i.e., similar trends between Cs_p and Cs_p/Th_p) though not always throughout the year (e.g., example of LR in 2014/2015, Fig. S3), and increased concentrations with SPM events, particularly at T and LR. This contrasts with the study from Evrard et al. (2015) who highlighted the relevance of particle size on the transport of radiocesium from the hilltops to the coast of Japan.

Overall, annual discharge-weighted fluxes show that the contribution of the Lot River into the Garonne River is low but significant in the dissolved phase. In fact, dissolved fluxes from the Lot River generally account for 70–135 % of that from the upstream Garonne River (T vs PSM). The influence of RM into the Lot River is <4 %, except in 2017 where it increased to 17 %, mainly in particulate form. Out of the studied rivers in this work, the upstream Garonne River contributes the most to the Cs influx into the Gironde Estuary, with >98 % as Cs_p.

3.1.2. Four contrasting hydrological conditions in the Gironde Estuary

Once in the estuary, Cs_d shows increased concentrations along the salinity gradient which could be confounded with a conservative behavior. However, a closer look at the results from MGTS II (flood conditions) and MGTS III (drought conditions) suggests a two-step increase in Cs_d, with an inflection point at S = 10 (Fig. 4). This inflection point is a physical-chemical response of Cs dynamics and not an anthropogenic influence given the variable location of the water mass of S = 10, i.e., for our sampling campaigns, S = 10 was positioned at KP61 during low discharge (260 m³ s⁻¹) and at KP90 during high discharge conditions (3450 m³ s⁻¹). Despite the incomplete dataset, the fluvial endmember at LR as well as reported seawater endmembers (Rankin,
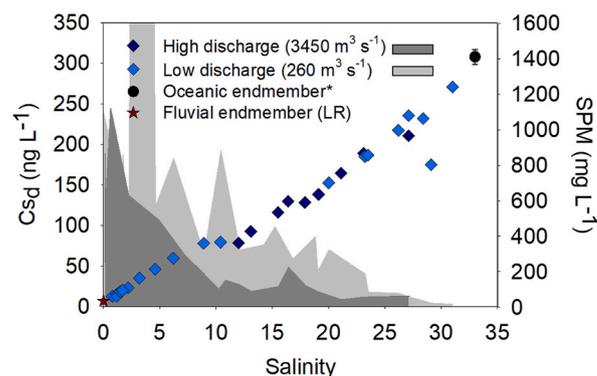

Fig. 4. Distribution of Cs_d (symbols) along the salinity and turbidity (shaded areas) gradients of the Gironde Estuary in flood (MGTS II – March 2015, 3450 m³ s⁻¹) and drought (MGTS III – October 2015, 260 m³ s⁻¹) conditions, sampled between the city of Bordeaux (Bdx_0 km) and the estuary mouth (C_110 km). Freshwater endmember is calculated from the 4-y timeseries at LR_Gar-70km (i.e., Fig. 3, error bar smaller than the symbol size) and the oceanic endmember corresponds to reported values in the literature (Rankin, 2009; Takata et al., 2013). Gray areas represent the SPM concentrations of corresponding campaigns.
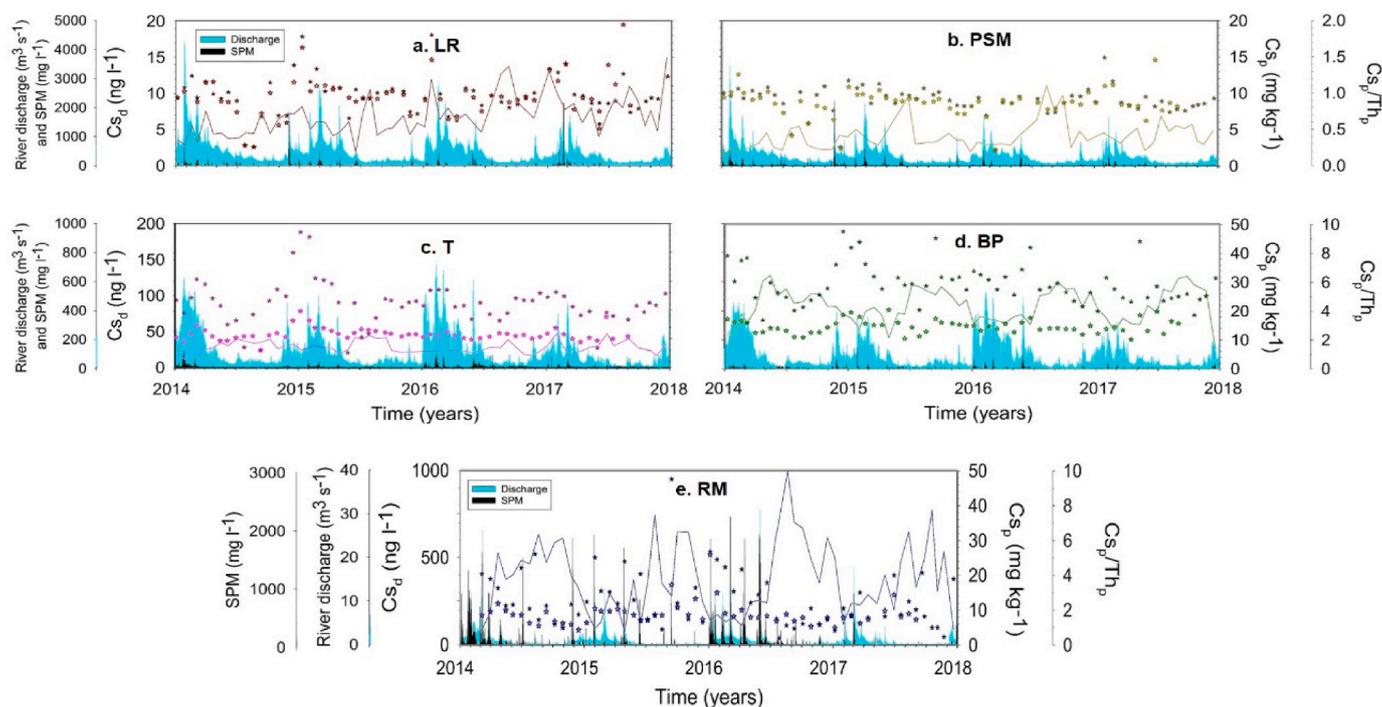

Fig. 3. Temporal variability of dissolved (Cs_d – lines), particulate (Cs_p – filled stars) and Th-normalized (Cs_p/Th_p – empty stars) cesium (Cs) concentrations in the Lot-Garonne fluvial system from 2014 to 2017 (4-years) at five sampling sites: La Réole (a, LR_Gar-70km), Port-Sainte-Marie (b, PSM_Gar-135km), Temple (c, T_Lot-135km), Boisse-Penchot (d, BP_Lot-235km) and Riou Mort (e, RM_Rio-250km). Corresponding water discharges are blue-shaded areas and suspended particulate matter (SPM) concentrations are also included. (For interpretation of the references to colour in this figure legend, the reader is referred to the Web version of this article.)

2009; Takata et al., 2013) contribute as reference points.

On the other hand, Cs_p shows a contrasting behavior depending on the water discharge conditions (Fig. 5). During flood conditions (e.g., MGTS I and MGTS II, Fig. 5a and b), Cs_p increases along the salinity and turbidity gradients of the Gironde Estuary, particularly at the MTZ where the highest SPM content is positioned. However, during drought conditions (e.g., MGTS III and MGTS IV, Fig. 5c and d), Cs_p decreases up to an average concentration of ~10 mg kg^{-1}. This behavior of Cs_p is not always an effect of changes in grain-size, as shown by the Cs_p/Th_p ratios. However, the decrease of coastal Cs_p up to 5.88 ± 0.73 mg kg^{-1}, seems to be related to grain size effects, reaching a coastal value of Cs_p/Th_p ~1.0 (i.e., specifically varying between 0.85 and 0.98).

3.2. 24 h cycle at the Gironde Estuary mouth

Given the dominance of the seawater endmember on Cs_d, only Cs_p was measured at the estuary mouth during a diel cycle in drought conditions (MGTS IV, Fig. 6). Results indicate that despite the diel cycling of seawater (salinity), SPM (i.e., remobilization with ebb and flood), and the day-night patterns (white vs gray area), Cs_p variations at the estuary mouth seem to be related to grain-size effects (i.e., the Cs_p peaks at night are smoothen with Cs_p/Th_p normalization). This trend is clearer when representing Cs_p vs Th_p trends (Fig. S3), particularly at the estuary mouth compared to the estuarine and freshwater areas. The Cs_p/Th_p ratios at the estuary mouth are generally within the coastal range (between 0.85 and 0.98, Fig. 5). The question then arises regarding the influence of such Cs_p dynamics on the bioaccumulation of Cs_b by wild oysters at the estuary mouth.

3.3. Historical trend in wild oysters at the estuary mouth

At first sight, the accumulation of Cs within the soft tissue of wild oysters at the estuary mouth shows a uniform concentration (1984–2010) followed by a significant increase in the last 4 years of the dataset (Fig. 7). This temporal distribution does not show a clear trend, as shown by several regression fits (i.e., Table S3). Nevertheless, the Cs_b distribution is not completely independent of the annual estuarine discharge (i.e., only showing inversely correlated anomalous points for
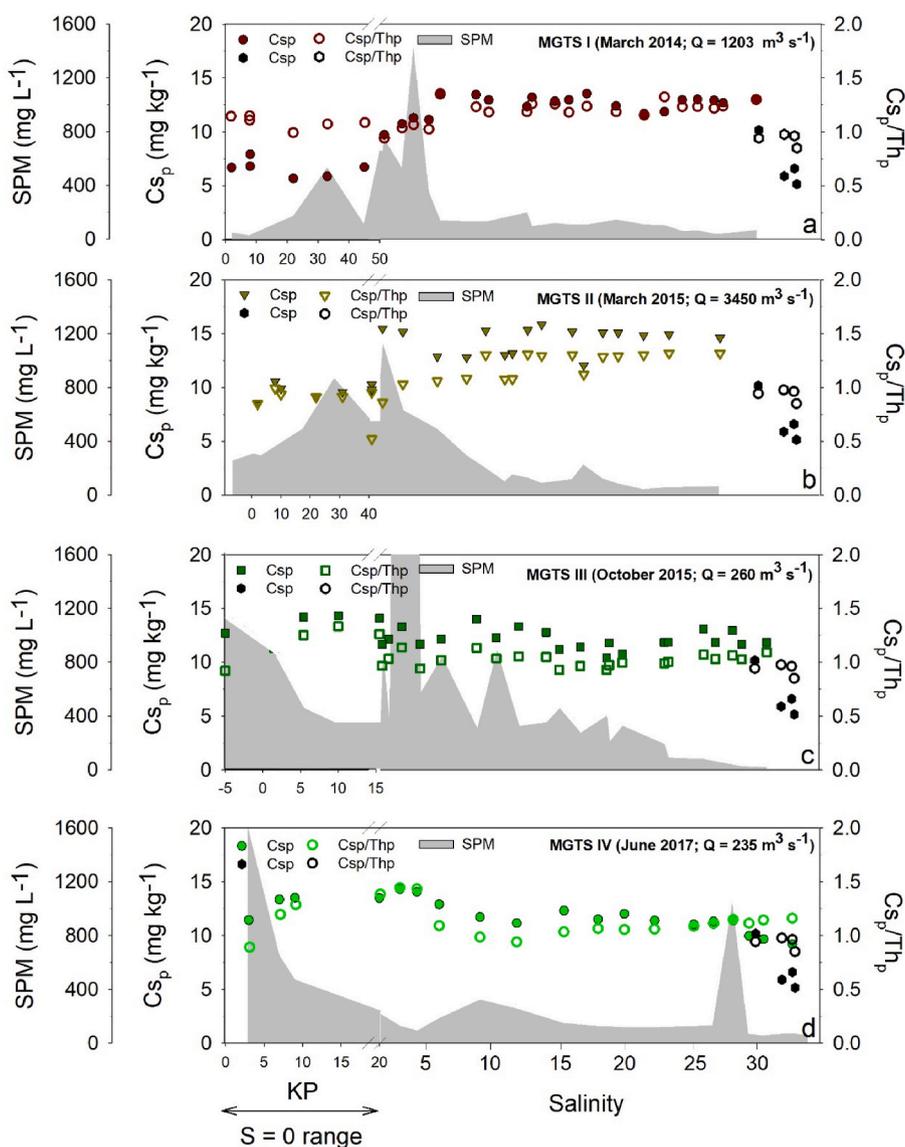

Fig. 5. Particulate (Cs_p) and Th-normalized (Cs_p/Th_p) concentrations of Cs along the estuarine salinity and turbidity gradients in the Gironde Estuary during four oceanographic sampling campaigns between the city of Bordeaux (Bdx_0 km) and the estuary mouth (C_110 km) during contrasting hydrological conditions: MGTS I (a), MGTS II (b), MGTS III (c), MGTS IV (d). Coastal Cs_p and Cs_p/Th_p values are presented in black. They were sampled during MGTS IV but it is shown for all conditions (a–d) as reference point for comparison. Suspended particulate matter (SPM concentrations, shaded gray) is also included.
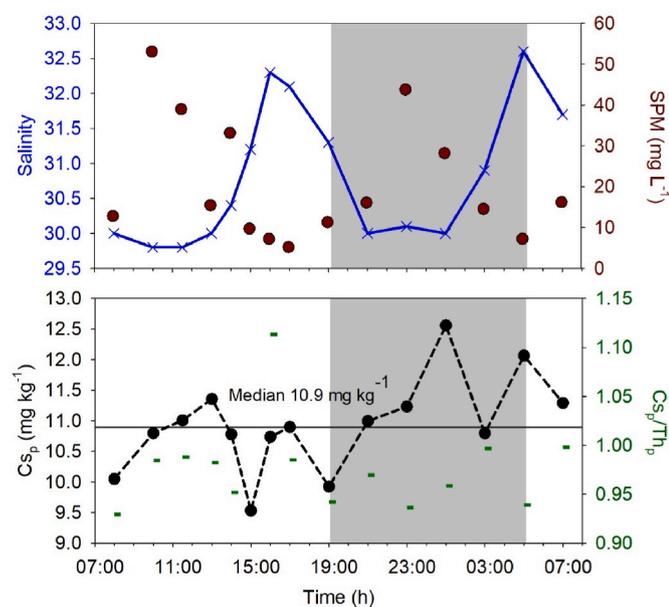
Fig. 6. 24 h cycle at the Gironde Estuary mouth (C_110 km) during drought conditions (MGTS IV, 235 m^3 s^{-1}) in June 2017. Median of Cs$_p$ concentrations is included (black line). Night-time is also indicated (gray area). Further physical-chemical and biological parameters of the cycle were published in Abdou and Tercier-Waeber (2022).
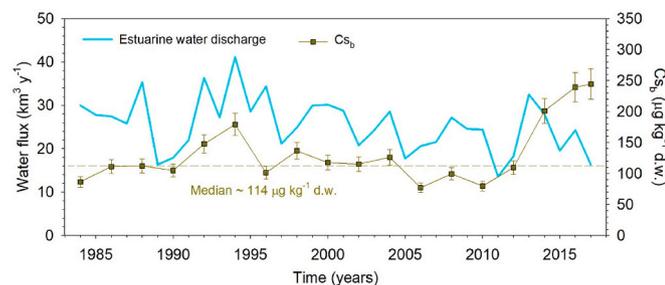

Fig. 7. 34-year historical trend of Cs accumulated in wild oysters at the Gironde Estuary mouth (LF_85 km). The median Cs concentration as well as the overall estuarine water discharge are included.

the last 4 years, as shown in the last row of Table S3). Regarding organotropism, out of the total Cs$_b$, average 55 % is accumulated in the mantle of the oysters and 27 % in the digestive gland (Fig. S1).

4. Discussion

4.1. Sources and watershed signal

Stable Cs is a lithophile element present between 1.0 and 3.7 mg kg^{-1} in the Earth's crust (Salminen et al., 2005). It is mainly present as a substitute of potassium (K) in mica and K-feldspars, showing the highest contents in pegmatite micas such as those found in Margeride granite of the Massif Central. Nevertheless, reported concentrations in stream sediments in Europe can reach 68 mg kg^{-1} locally. Stream water on the other side, has a median of 6 ng L^{-1} with point sources of up to 24 000 ng L^{-1} in some countries (Salminen et al., 2005). This work reports average concentrations and Kd values for the Lot-Garonne-Gironde fluvial estuarine system (Table 3). These concentrations fall within the expected environmental ranges, even for estuarine systems. In fact, apart from the aforementioned punctual Cs$_d$ and Cs$_p$ from hydrological surveys and to the best of our knowledge, there are only three studies focusing on stable Cs in estuarine environments (Shim et al., 2012; Takata et al., 2013; Bera et al., 2015). The

first two studies also found Cs$_d$ ~12 ng L^{-1} for the freshwater endmembers and ~308–316 ng L^{-1} at the seawater endmember off the coast of Japan (i.e., Kako and Kitakami rivers; Takata et al., 2013) and in the Gulf of Mexico (i.e., Mississippi River outflow; Shim et al., 2012). The third study, also conducted in the Gulf of Mexico (i.e., St. Louis Bay; Bera et al., 2015) actually showed signs of contamination (i.e., Cs$_p$: 0.07–50 mg kg^{-1} in SPM, Cs$_d$: 0.13–6.65 µg L^{-1}, reaching punctually max. Values of ~16.3 and ~53.2 µg L^{-1} related to the outfall of a nearby titanium dioxide refinery using Cs salts as a nucleant). These studies relativize the levels found in the Lot-Garonne-Gironde fluvial-estuarine continuum, suggesting a non-anthropized signal of Cs from the watershed.

Stable Cs has relatively few anthropogenic uses and applications (e. g., primarily for oil and gas well drilling, in photo-electronic cells and detectors of scientific instruments; USGS, 2022). Therefore, most Cs environmental signals are associated to erosion/weathering products from natural rocks (Salminen et al., 2005). In fact, Spearman correlations between the parameters per site (Table S4) show significant correlations (p_value < 0.05) for Cs$_d$ with SPM and for Cs$_p$ with water discharges for all sites. This seems to indicate a Cs$_d$ controlled system where watershed erosion releases soluble and easily transported Cs into the aquatic system, which subsequently adsorbs Cs along the river pathway onto its slower moving SPM. Thus, reported Cs concentrations in the Lot-Garonne-Gironde fluvial-estuarine system (Fig. 3) are linked to a direct signal from the watershed rock composition. That is, in this study, we have observed three main Cs$_p$ sources with the following decreasing Cs content: Massif Central > Pyrenean Mountains > RM watershed. The difference in Cs concentrations between BP and RM highlights this hypothesis, as both sites derived from different rock sources within the Lot River watershed. The Massif Central (i.e., main contributor of SPM at BP) contains strong Cs enrichments in Hercynian leucogranite intrusions and Cs-rich fluorine mineral ores (BRGM, 1978; BRGM, 1983; Salminen et al., 2005). At intermediate Cs levels, the upstream Garonne River (i.e., PSM) is under the influence from the Pyrenean Mountains and from of sands and clays along the watershed (BRGM, 2014). On the other hand, the Riou Mort River watershed in itself (i.e., RM site) mainly contains conglomerates, sandstones and mudstones, with Permian argillite with high mica content, granite areas and some intercalations of pelites from the Carboniferous and coal seams/layers (Coynel et al., 2009). However, in terms of fluxes, the highest contributor of Cs$_p$ to the Gironde Estuary in this work is the upstream Garonne River (c.f., Cs$_p$ fluxes, Table 2). The lower influence of discharge-weighed Cs$_p$ fluxes from the Lot River into the Garonne River could be related (i) to the fact that the erosion in the Lot River are weaker than in the Garonne River, and (ii) that several dams are located along the Lot River which can retain part of the carried SPM. The influence of the Dordogne and Isle rivers (Fig. 1) have not been studied in this work but should not be underestimated, given the fact that these rivers are also sourced in the Massif Central and may contain high erosion and/or less dams along their course (i.e., average freshwater discharge for the past 60 years for the Dordogne River ~313 m^3 s^{-1} vs Garonne River ~586 m^3 s^{-1}, DIREN, 2023, and Table 2 for annual water fluxes).

On the other hand, Cs$_d$ from RM showed the highest concentrations in the system. However, its source is yet unknown, as the low Cs$_p$ concentrations at the RM watershed do not seem to explain this contrast. This could be related to a low water discharge (i.e., low dilution factor) and/or alternative uses of Cs in the area. For example, cesium salts can be used in water treatment facilities (USGS, 2022). Past remediation works performed at the RM watershed, or the nearby wastewater treatment plant and companies could have used/be using Cs containing products. To the best of our knowledge, there is no information about the impact of such works at RM on Cs dynamics and further research should clarify this point. Nevertheless, the influence of Cs$_d$ fluxes from the RM watershed into the Lot River is generally low (Table 2). Along the Lot River, there is a decrease in Cs$_d$ between BP and T, which could be related to the inflow of different rivers and/or to rapid sorption of Cs

Table 2
Annual discharge-weighed fluxes along the Lot-Garonne fluvial system from 2014 to 2017 (4-years) at five sampling sites: La Réole (LR_Gar-70km), Port-Sainte-Marie (PSM_Gar-135km), Temple (T_Lot-135km), Boisse-Penchot (BP_Lot-235km) and Riou Mort (RM_Rio-250km). Reported fluxes include water discharges (F_Q, km³ y⁻¹), SPM (F_{SPM}, Mt y⁻¹), dissolved (F_{Csd}) and particulate (F_{Csp}) fluxes for Cs.

Year	LR	PSM	T	BP	RM
F_Q (km³ y⁻¹)					
2014	20.0	14.0	4.70	3.70	0.05
2015	14.0	10.5	3.00	2.20	0.03
2016	15.5	9.70	5.00	3.90	0.05
2017	10.7	7.90	2.50	2.20	0.03
F_{SPM} (Mt y⁻¹)					
2014	1.80	1.55	0.11	0.03	0.02
2015	0.85	0.80	0.04	0.02	0.01
2016	0.75	0.50	0.12	0.04	0.03
2017	0.60	0.30	0.04	0.01	0.01
F_{Csd} (kg y⁻¹)					
2014	77.4	35.5	105	260	6.88
2015	78.6	22.8	56.5	170	4.56
2016	112	34.4	117	280	10.4
2017	82.6	29.6	73.6	170	7.18
F_{Csp} (kg y⁻¹)					
2014	24 500	22 850	2710	867	7.23
2015	10 810	8140	1310	360	47.5
2016	3680	1340	1750	610	35.6
2017	2060	2780	206	925	39.4

onto SPM, as pointed out by the Spearman correlations (Table S4), i.e., Cs released from weathered rocks and minerals is known to rapidly adsorb, especially onto clays (Kabata-Pendias, 2011). For instance, downstream the Lot River (i.e., location of T), surface rocks contain clays but, most importantly, the location of a dam increases the retention of fine particles and the residence times of exchange, which can potentially explain the factor 3 decrease of Cs_d. The even lower Cs_d levels found upstream the Garonne River can be related to different Cs rock sources and/or to a longer transport time along the Garonne River where clays/sands (BRGM, 2014) adsorb more Cs_d than the shorter pathway of the Lot River. In fact, sorption of Cs seems to occur quite readily, as the sum of annual Cs_d fluxes at PSM and T are not retrieved at LR for the same year (i.e., except for the year 2015, consistent water discharges and addition of SPM load between PSM + T and LR cause a systematic loss of Cs_d annual fluxes, Table 2). Therefore, despite the high influence of the Lot River in the Cs_d budget of the Garonne River, often almost half of it is adsorbed onto the particulate phase before reaching the Gironde Estuary.

4.2. Known sorption mechanisms of Cs onto environmental surfaces

4.2.1. The importance of clay minerals

The scientific literature contains extensive research on the sorption mechanisms of Cs, particularly oriented towards the context of nuclear waste disposal and potential radionuclide migration from deep geological sites. It is well recognized since the 1970's that clay minerals are the most important mineral phase for adsorption of (radio)cesium, with illite being the most predominant, most studied and the clay type presenting the highest sorption affinity out of all studied minerals (Comans and Hockley, 1992 and references therein). Other clay minerals such as kaolinite, smectite and vermiculite can also play an active role (Naulier et al., 2017; Okumura et al., 2018; Delaval et al., 2020) but are generally less studied. Alternative surfaces such as TiO_2 engineered nanoparticles (Metwally et al., 2007), iron oxides (magnetite, ferrite; Sheha and Metwally, 2007) or humic acids (Khan and Bagla, 2022) are seldomly investigated and are more focused within the context of remediation and treatment of radioactive liquid waste. A summary of the experimental conditions and obtained Kd values for experimental, single mineral-based studies (Table S5), relativizes and brings forth the relevance of clay minerals over other surfaces regarding Cs sorption.

The main mechanisms for Cs sorption onto clay minerals are related to their varied and densely distributed surface binding sites. Clay minerals in general show a platelet-like form with planar areas (negatively charged on a permanent basis), edge areas (i.e., edge or frayed-edge sites, with pH-dependent varying charge), and interlayered sites involved in sorption processes. Planar sites can form strong inner-sphere complexes absorbing efficiently monovalent cations like K^+, Cs^+, Rb^+, etc., within a few hours (Onishi et al., 1981; Comans and Hockley, 1992; Wauters et al., 1996; Poinssot et al., 1999; Sposito et al., 1999; Bayülken et al., 2011; Nakao et al., 2014). Sorption on the weathering sites of micaceous minerals (edges, frayed-edges and interlayers) also occur for low hydration monovalent cations, like Cs^+ as their effective ionic radii is small enough to access these sites compared to more hydrated ions (e. g., Li^+, Na^+, etc.; Zachara et al., 2002). Nevertheless, it is generally considered that both planar and interlayer sorption may be partially reversible with increasing ionic strength (i.e., competitive K^+, Na^+ or NH_4^+ in reducing conditions) favoring the release of Cs^+ into the dissolved phase (Delaval et al., 2020).

4.2.2. Existing models for Cs sorption onto clay minerals (illite, smectite and kaolin clay groups)

There are several works characterizing and modeling Cs sorption mechanisms onto clay minerals. Many of these simplify the process to a purely based cation exchange mechanism (i.e., no inner sphere complexation) involving monovalent cations and illite. Probably, one of the most cited works in this field are those from the group of Bradbury and Baeyens (2000). They suggest a cation-exchange generalized model accounting for $Cs^+/Na^+/K^+/Rb^+/NH_4^+$ exchanges onto a "reference illite" at equilibrium conditions based on various experimental evidences with several illitic clays (saturated in Ca, Sr, Ba, Na or K ions; Brouwer et al., 1983; Poinssot et al., 1999; Baeyens and Bradbury, 2004). Their cation-exchange model describes three types of functional sites (presented in Table S2): frayed-edge sites (FES, with a low exchange capacity of ~0.5 % but exclusively enthalpic and highly selective for Cs, particularly at low concentrations), type-II sites (~20 % of the exchange capacity) and planar sites (with ~80 % of the total exchange capacity but no significant affinity for Cs). Some works report that a two-site model including FES and type-II sites is often sufficient to

Table 3
Average ± SD values (N > 30) for all the datasets presented in this work regarding dissolved (Cs_d, ng L⁻¹), particulate (Cs_p, mg kg⁻¹) and $\log_{10}$ Kd (L kg⁻¹) values of Cs at each fluvial site and within the estuary at the Lot-Garonne-Gironde fluvial-estuarine system. Range of values are reported for SPM concentrations (mg L⁻¹) at all sites as well as for Cs_d within the estuary. Fluvial sites correspond to: La Réole (LR_Gar-70km), Port-Sainte-Marie (PSM_Gar-135km), Temple (T_Lot-135km), Boisse-Penchot (BP_Lot-235km) and Riou Mort (RM_Rio-250km). Values presented for the Gironde Estuary correspond to results between Bdx_0 km and C_110 km. The Cs_d values of the oceanic endmember correspond to the literature (Rankin, 2009; Takata et al., 2013), whereas the Cs_p come from the most coastal points in this work (shown in Fig. 5).

Sites	RM	BP	T	PSM	LR	Gironde Estuary	Coastal values
Cs_d	366 ± 219	87.6 ± 23.6	28.4 ± 8.2	3.99 ± 1.95	6.81 ± 2.72	12.8–271	307 ± 9.10
Cs_p	13.0 ± 7.9	29.8 ± 7.3	22.2 ± 7.6	9.01 ± 2.0	9.77 ± 2.68	12.3 ± 1.78	6.96 ± 2.23
$\log_{10}$ Kd	4.54 ± 0.48	5.54 ± 0.20	5.87 ± 0.24	6.38 ± 0.24	6.17 ± 0.20	5.20 ± 0.44	4.37 ± 0.23
SPM	1–690	<1–39	1–68	1–386	1–177	18–890	6.40–10.3

reproduce the experimental data related to radioactive waste disposal on a wide range of pH and ionic strength (Poinssot et al., 1999). Only when concentrations of Cs are above 0.0003 M (~40 mg L^{-1}, way beyond natural concentrations) the third site (i.e., the planar site) is required, at least applicable for studies with illite du Puy (Poinssot et al., 1999). The reproducibility of this cation-exchange model has been validated on weathered clays by other techniques such as molecular dynamics (e.g., Zaunbrecher et al., 2015).

The role of smectite clay-types on Cs sorption has also been studied (Gutierrez and Fuentes, 1996; Iijima et al., 2010; Missana et al., 2014). Missana et al. (2014) developed a two-site cation exchange model for smectites (edge and planar, also included in Table S2) by fitting the experimental data to realistic conditions; three homo-ionic smectites (Na-, K-, Ca-smectite), in a wide pH range (2–11), at varying ionic strength (0.001 M–1 M) and Cs concentrations (10^{-10} – 10^{-3} M, i.e., ~13.7 ng L^{-1} to 137 mg L^{-1}). Other studies highlight that cation-exchange processes are not enough to explain Cs sorption onto montmorillonites. For instance, Iijima et al. (2010) suggested that, at basic pH (8 and 10), sorption of Cs (10^{-11} – 10^{-5} M) was mainly dominated by ion exchange (one-site model based on FES) but a surface complexation model was also required to explain the nanoparticle size effect. Gutierrez and Fuentes (1996) took a step forward and defined a triple layer model (TLM, electrochemical adsorption model) for quantifying Cs sorption onto Ca-montmorillonite, in the presence of Sr^{2+} competition. The TLM was based on two sorption sites (interlayer and FES) and model parameters were fit to experimental conditions mainly focused on freshwater systems (20 g L^{-1} of solid/liquid ratio, in 0.001 M NaCl, at adjusted pH between 4 and 9). Despite the reported Cs strong sorption (75–88 %) and low irreversibility, their Cs concentrations were quite beyond natural conditions (i.e., between 0.94 and 4.29 mM, which corresponds to ~125 mg L^{-1} – 570 mg L^{-1}) and the authors even mentioned that CsOH precipitation could not be discarded in some cases.

4.2.3. Modeling Cs sorption within the Gironde Estuary

Before modeling any sorption conditions, one should bear in mind that many models are based on equilibrium conditions and kinetics are taken into account only when explicitly defined. In general, one should not underestimate the role of kinetics during sorption, as both different clay sites (e.g., FES takes 5 days to reach equilibrium compared to type-II sites within a few hours; Poinssot et al., 1999) or clay types (e.g., Ca-illite surfaces show slower uptake of Cs compared to K-illite; Comans and Hockley, 1992) may show kinetic reactivity. The environmental dynamics and residence times of water and particles may also vary quantitatively Cs sorption compared to expected scenarios based on equilibrium conditions (Comans and Hockley, 1992). This idea of kinetically influenced sorption based on residence times is actually included nowadays as a two-step kinetic submodel (i.e., exchangeable vs fixed sites) within the main code of radionuclide dispersion models (based on equilibrium Kds). The latter has been validated and used for predicting the dispersion of ^{137}Cs in Japanese rivers after the Fukushima Dai-ichi NPP accident in 2011 (Zheleznyak et al., 2022). Nevertheless, this kinetic aspect is incorporated as an option and not a regular routine, for reducing computational efforts and because kinetic effects are only considered significant when freshwater systems show particle residence times of a few days. This means that in most cases, equilibrium conditions are assumed to be achieved (i.e., applicable for the experimental conditions in Comans and Hockley, 1992). Thus, given the residence times of water and SPM within the Gironde Estuary (*c.f.*, section 2.1), we assume that equilibrium conditions are reached within its salinity and turbidity gradients.

Model results confirm that the observed Cs$_d$ pattern along the salinity gradient deviates from the conservative behavior (Model 1, Fig. 8a). In fact, it shows that the Gironde Estuary is acting as a sink or scavenged system for Cs$_d$, contrary to what one would think when only observing field results like in Fig. 4. For instance, it has been shown experimentally
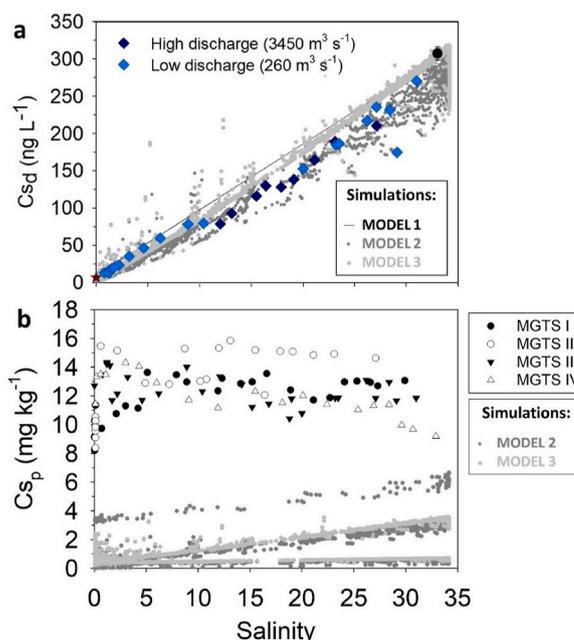

Fig. 8. Model output showing cation-exchangeable (a) Cs$_d$ and (b) Cs$_p$ reactivity for the simulated conditions (Model 1–3). In both cases, field Cs$_d$ and total particulate Cs$_p$ (presented in Figs. 4 and 5 for sampled points between Bdx_0 km and C_110 km) are overlayed for comparison. As a reminder: Model 1 simulates the conservative behavior, Model 2 Cs reactivity via cation-exchange on fresh SPM, and Model 3 Cs reactivity via cation-exchange on old SPM.

that Cs desorption always shows a plateau of desorption in solutions when only K$^+$ increases in concentration (tested for 10^{-5} to 1.6 M of K$^+$, equivalent to a salinity range from freshwater to brine composition) but shows linear, though lower, desorption with Na$^+$ increases (Desai et al., 1994; Onodera et al., 2017; Mukai et al., 2018). Thus, one could have identified the plateau at S = 10 as an effect of Cs within the MTZ due to the influence of increasing K$^+$, followed by a conservative mixing between 10 < S < 35. However, Model 1 suggests that no sorption (ad- nor de-sorption) takes place at S < 10. Models 2 and 3 show that for S < 10, "old SPM" particles do not adsorb anymore Cs, associated to the position of the MTZ (displayed in Fig. 4). Beyond S > 10 "fresh SPM" acts as an overall sink for Cs$_d$, deviating from the conservative line and explaining the behavior of falsely observed outliers too (e.g., point at S = 30, Fig. 8a). This is the first environmental study to report a visible plateau at S = 10 which is not related to Cs desorption, i.e., Cs$_d$ concentrations at S > 10 are below the expected physical mixing of water masses, which means that there is a sink of Cs$_d$ in the system as Cs adsorbs onto the SPM. These results contrast to reported experimental laboratory observations identifying a desorption threshold between S = 10–15 (Delaval et al., 2020). Field works have reported less clear reactivities for Cs in other systems: unclear at the Kako and Kitakami rivers due to few sampling points (Takata et al., 2013), conservative behavior in the Mississippi River outflow (Shim et al., 2012), and highly modified at the St. Louis Bay due to the high influence of anthropogenic sources, despite the several sampling campaigns reported during different years and seasons (Bera et al., 2015). Several explanations exist for the reported differences in non-contaminated estuaries: (1) analytical precision (though unlikely, SF-ICP-MS vs TQ-ICP-MS), (2) mineral composition (even though the Mississippi River is known to contain clay minerals), and (3) the SPM concentration. The latter two might be the determining factor, as the average SPM in the Gironde Estuary has a similar order of magnitude to the reported SPM values of the Mississippi River (clay fraction of 100–400 mg L^{-1}; Hanor and Chan, 1977). Furthermore, studies on radioactive Cs (^{137}Cs) have shown desorption behavior due to increased salinity in the Hudson River for SPM ~ 40–200 mg L^{-1} as well

as in deep sediments of the San Francisco Bay (Olsen et al., 1981; Volpe et al., 2002). Thus, it seems that for the Gironde Estuary, SPM mineralogy together with its reactivity and the highly concentrated MTZ cause the observed plateau.

The modeled Cs_p (Fig. 8b) seems far away from the observations. However, field Cs_p withholds all the geogenic Cs content, as total digestions were performed on these samples, and the model only provides the cation-exchangeable fraction on the simulated SPM. Aqua regia digestions performed in the estuarine SPM (data not shown) back up this hypothesis, where only 55 % of the total Cs was extracted. This means that, for the modeled conditions, Cs reactivity within the Gironde Estuary can be explained by the clay fraction (i.e., both illite and smectite contributions), even though it accounts for <45 % of the total mineral SPM content (Gil-Díaz et al., 2020). Noteworthy, the increasing Cs_p trend along the salinity gradient shown by both models is not directly comparable to field observations (e.g., more horizontal trend) because the SPM inside the simulated MTZ is not mobile and in reality, there is also an influence from oceanic SPM.

In addition, the accumulation of Cs within the full modeled column (Fig. 9, modeled water discharge conditions presented in Fig. S2) also shows that in both Model 2 and 3, overall Cs adsorption onto SPM within the estuary can also occur during seawater intrusion (drought events), and Cs desorption during freshwater influence (as a re-equilibration effect to lower Cs_d concentrations, Fig. 9c and d). These high variations in salinity (from 0 to 35) show significant changes on the total column/estuarine Cs_p content. Only during long flood periods (Fig. 9d), Cs also adsorbs during freshwater intrusion, as observed on Cs_p during MGTS I and II (Fig. 5). During full drought events, only a maximum accumulation of Cs_p is reached (Fig. 9d), despite the SPM not being fully saturated (i.e., the illite and smectite functional sites are <12 % occupied), and desorption takes place due to freshwater tidal influence (i.e., Cs species exchanges along the simulated column during drought conditions is shown in Fig. S4), potentially comparable to observations during MGTS III and IV (Fig. 5). Noteworthy, simulations only consider the equivalent dynamics of "truly dissolved" Cs species, i.e., distribution of total Cs into free ions (Cs^+), chlorinated forms (CsCl) and hydroxyl forms (CsOH), based on the thermodynamic information provided by the PhreeqC database. In any case, these simulations indicate that Cs sorption is strongly related to ionic strength (and Cs_d endmember concentrations), explaining why small variations on salinity (between 30 and 32) did not show a clear Cs_p cycle at the estuary mouth (Fig. 6). However, SPM can desorb Cs_p over time once released into the coastal areas, where the freshwater influence is lower and the more strongly

bound Cs can be extracted. The difference between the ion-exchange budget (modeled, Fig. 8b) and the geogenic component (non-exchangeable fraction) could give the signal observed in the coastal SPM (Fig. 5).

4.3. Reactivity along the fluvial-estuarine system

4.3.1. Seasonal variability

Despite the different characteristic concentrations along the Lot-Garonne fluvial system, Cs_p and Cs_d show seasonal variations. Based on our observations, this variability could be likely related to erosion/remobilization of SPM and dilution effects. These variations are also transferred to the Kd values, showing different seasonal patterns along the year depending on the fluvial site (Fig. S5). Even though a longer temporal series could establish a more robust pattern, some sites (e.g., RM, BP, T and PSM) seem to show low relative $\log_{10}$ Kd values at different months of the year. For example, RM shows the lowest $\log_{10}$ Kd values from August to October, whereas for T this solubility appears earlier in the year (during June to August) and for PSM somewhere in between (during July to September). These seasonal variations however are not as pronounced as those found for Te (Gil-Díaz et al., 2019), Sb (Gil-Díaz et al., 2018), As (Masson et al., 2007), Mo and V (Masson, 2007), also detected at the same sites. The temporal variability of these metalloids was attributed mainly to redox processes (e.g., related to microorganism activities, directly or via mineral dissolution), particularly for Sb and As. Alternatively, a combination of weathering effects from silicate rocks (*c.f. section 4.1*; e.g., Te and V; Schiller and Mao, 2000; Gil-Díaz et al., 2019) and secondarily *in situ* redox changes may also be involved in the observed seasonality (e.g., Mo and V case for Mississippi River; Shiller, 1997; Shiller and Mao, 1999). For example, after the Fukushima accident, changes in land elevation and subsequent erosion were identified as a relevant factor for $^{137}Cs_p$ transport in the Niida River (Wakiyama et al., 2022). In addition to rock weathering, rivers may also receive elements along the year from several/different sources including groundwater fluctuations.

Alternatively, biological activities and/or temperature related thermodynamics, could also explain Cs seasonality in aquatic systems. For instance, after the Fukushima accident, Cs_p, Cs_d and Kd values from released ^{137}Cs into the urban river of Harai between 2014 and 2019 showed mild seasonal patterns (Nanba et al., 2022). Only these samples from the Harai River showed correlation was between $^{137}Cs_d$ and the water temperature (Nanba et al., 2022). Our study shows a correlation between $\log_{10}$ Kd of stable Cs and water temperature for the sites at the
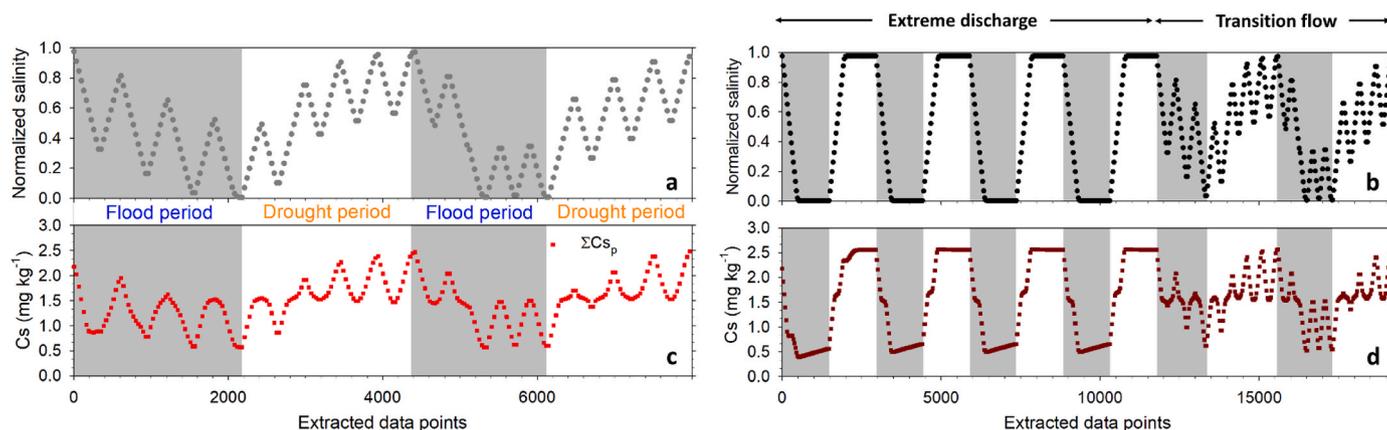

Fig. 9. Overview of the full column behavior during Model 2 (a,c) and Model 3 (b,d), as described in Table 1 and Fig. S2. The X axis represents extracted information for the whole column over the simulation time. Panels (a, b) show the average salt content present in the column, via a normalized salinity value. Normalized salinity corresponds to the $\Sigma Si/(35 \cdot i)$, where i is the number of modeled cells (i = 30) and 35 is the salinity of the simulated seawater endmember. This means that 1.0 corresponds to a column filled with seawater of salinity 35, and 0.0 to a column full of freshwater. Panels (c,d) show the total average Cs_p content within the column. White areas are seawater intrusion events in the column (simulating drought periods). Correspondingly, gray areas show freshwater intrusion (simulating flood periods).

Lot River (strongest at RM - not shown, followed by T and less evident at BP; Fig. S6). Noteworthy, the same dependency is found between the $\log_{10}$ Kd As vs water temperature (slope of -0.027 ± 0.002, Fig. S6c) and that of $\log_{10}$ Kd Cs vs water temperature at Temple (slope of -0.026 ± 0.003, Fig. S6d). This could imply that either Cs is related to thermodynamics and As to biological activity, which occur at the same rate due to temperature correlation, or that biological activities actually affect both element dynamics. Given the lack of organic data for our studied system and the order of magnitude of Cs Kd values with humic substances (i.e., Table S5, Khan and Bagla, 2022), one should not discard the potential influence of organic matter, e.g., coating the SPM, on Cs seasonal variability in freshwater systems. Nevertheless, further studies are required to verify the processes behind these correlations. In any case, similarities between stable and radioactive Cs in seasonal response indicates (i) that environmental factors apply to both inherent and added Cs (as hypothesized), and therefore (ii) local environmental dynamics of stable Cs can provide valuable understanding of Cs reactivity in aquatic systems, relevant for post-accidental management strategies before the accident takes place.

4.3.2. Watershed solid-liquid partitioning

Given the characteristic Cs_p and Cs_d found along the Lot-Garonne-Gironde fluvial-estuarine system, the solid-liquid partitioning of natural Cs (i.e., including all carrier phases from total digestions) varies at most 2 orders of magnitude along the watershed. Results show contrasting average $\log_{10}$ Kd values among upstream sources of Cs within the fluvial sites of the Garonne watershed (Table 3), but relatively constant average $\log_{10}$ Kd values along the Lot-Garonne continuum (i.e., from 5.87 L kg^{-1} at T to 6.17 L kg^{-1} at LR). Only when individual values are compared (Fig. 10) one can observe a slight increase on the $\log_{10}$ Kd values from BP to LR, in accordance with the sorption of Cs along the freshwater transport times of the Lot-Garonne River. The $\log_{10}$ Kd values decrease within the salinity and turbidity gradients of the Gironde Estuary to average 5.20 L kg^{-1} (Table 3), even though the latter is a result from the high Cs_d influence from the oceanic endmember ($Cs_d \sim 300$ ng L^{-1}).

The overall range of $\log_{10}$ Kd values is slightly higher than reported $\log_{10}$ Kd in the literature, varying from 3.82 to 5.13 L kg^{-1} in freshwater and 2.65–3.30 L kg^{-1} in seawater (IAEA, 2004; Tagami and Uchida, 2013; Tomczak et al., 2019). However, it is difficult to generalize a comparison between Kd values when these are known to depend on
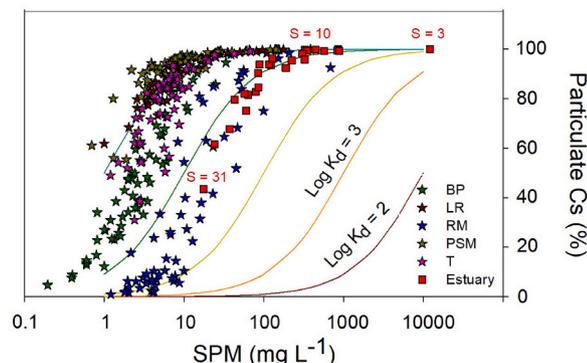
many factors (e.g., pH, mineralogy, ionic strength, solution composition, etc.) which vary between sites and added vs inherent elements. For instance, tracer experiments (*ex-situ* or *in-situ*) determine the Kd values only based on the added fraction of Cs, which might behave differently (e.g., more related to exchangeable fractions) than inherent Cs (i.e., also included in the refractory fraction, thus contributing with higher Cs_p for the calculation of the natural Kd values). This doesn't imply that added Cs will always show low Kd values, as evidenced for instance in the Harai River between 2014 and 2019, years after the Fukushima accident, showing constant average $\log_{10}$ Kd of 5.72 L kg^{-1} for ^{137}Cs (Nanba et al., 2022). A review on freshwater Kd values includes SPM concentration as a parameter based on *in situ* observations (Tomczak et al., 2019). For the case of the Lot-Garonne-Gironde fluvial-estuarine system, SPM concentration and age also affects the solid/liquid partitioning of Cs (e.g., Fig. 10, where the trends deviate from the theoretical Kd lines). Another factor that should also be included in the Kd variability of Cs is land use, as the higher Kds found in Fukushima are thought to be related to a higher $^{137}Cs_p$ transport due to urban impermeable surfaces (Nanba et al., 2022).

4.3.3. Modeling estuarine partitioning

It is a common practice in the literature that Cs dispersion models in coastal and river systems are based primarily on Kd values. This approach reduces/optimizes computational efforts by not incorporating the geochemical components, as done in this work. In order to predict Cs reactivity based on the Kd value, many dispersion models assume a single dependence of Kd to salinity (e.g., Periáñez, 2005; Zheleznyak et al., 2022). This means that Cs reactivity from Kd values is calculated along a given salinity gradient via a Langmuir isotherm. The equation was defined by Laissaoui et al. (1998), designed for reproducing sorption of a small amount of tracer at equilibrium, i.e., without further saturation of the SPM. The equation itself (Eq. (4)) only requires the Kd value of the freshwater endmember (Kd^{fw}) and the salinity value (S_0) at which the fraction of occupied sites on the SPM is 50 %.

$$Kd = Kd^{fw}\left(\frac{S_0}{S + S_0}\right) \tag{4}$$

In Fig. 11, we compare the field Kd data (MGTS II and III) with the modeled Kd values from Models 2 and 3, and the outputs for two adjusted S_0 values using Eq. (4). When plotting the Kd values obtained from Model 2 and 3 against the salinity, two main patterns appear. The difference in both trends is related to the Kd signal at the average 100 mg L^{-1} SPM vs the MTZ simulated area (1000 mg L^{-1}), which in the models it is immobile SPM in the simulated column. Nevertheless, the

Fig. 10. Distribution of the Cs_p content (%) out of the total Cs in the samples along the SPM concentrations in the Lot-Garonne-Gironde fluvial-estuarine system during 4-years of monitoring (stars) and 2 hydrological conditions (squares) along the salinity gradient (i.e., indicated in red). The corresponding salinities for the estuarine points are also included. Fluvial sites correspond to: La Réole (LR_Gar-70km), Port-Sainte-Marie (PSM_Gar-135km), Temple (T_Lot-135km), Boisse-Penchot (BP_Lot-235km) and Riou Mort (RM_Rio-250km). Estuarine values were calculated from the results between Bdx_0 km and C_110 km. (For interpretation of the references to colour in this figure legend, the reader is referred to the Web version of this article.)
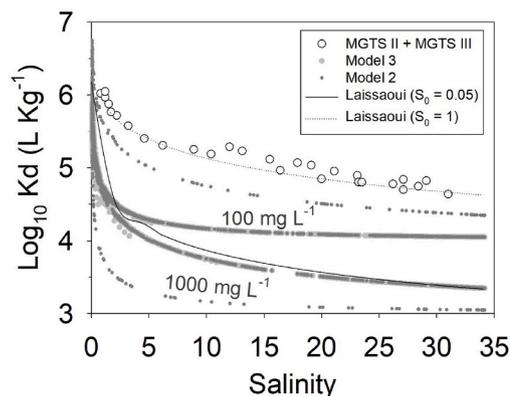

Fig. 11. Estuarine $\log_{10}$ Kd values along the salinity gradient. Field data from sampling campaigns (MGTS II and MGTS III, from sampling points between Bdx_0 km and C_110 km) are plotted together with PhreeqC modeled results (Model 2 and 3, simulating fresh and old SPM cation-exchange interactions) as well as with calculated Kd curves from Laissaoui et al. (1998) for two fitted S_0 values.

trend along the salinity gradient resembles that of field observations. Differences between the field and modeled data are related to the log scale and the fact that field Kd values include total Cs_p content whereas modeled Cs_p corresponds only to the exchangeable fraction (the relevant fraction for ^{137}Cs post-accidental modeling). The Kd trend obtained when using Eq. (4) and $S_0 = 1$ resembles quite well to field observations (based on total Cs_p) whereas a lower value (i.e., $S_0 = 0.05$) would fit better to the signal from 1000 mg L^{-1} SPM. These results mean that at S = 1, 50 % of the exchangeable sites from fresh SPM are occupied by Cs whereas in the MTZ this happens already at S = 0.05. However, Model 2 and 3 show that the overall site occupation in the simulated estuary is <16 %. These comparisons point towards the fact that Eq. (4) might be a fortuitus coincidence, as it was originally derived from sorption experiments based on $^{133}Ba^{2+}$ and is indiscriminately used for any other radionuclide/element reactivity. However, Eq. (4) cannot provide reasonable element-dependent information, as S_0 is the only unknown variable in the equation, and this can be manually fitted to field observations (which are normally based on total Cs_p and not only exchangeable Cs_p). Therefore, studies with specific elements (e.g., sorption with Cs) are necessary to clarify the application and meaning of Eq. (4) in dispersion models in order to provide reliable post-accidental measures.

4.4. Bioconcentration at the estuary mouth

This is the first work presenting the historical accumulation of stable Cs in wild oysters at the Gironde Estuary (Fig. 7). Results show a relatively stable bioaccumulation of total Cs_b over time, with a general correlation to the water discharge for most of the temporal series (i.e., p_value < 0.05 for the slope, Table S3). This could indicate an overall natural source of Cs to the wild oysters, with only three anomalous events in the last years of series (2014–2017, Table S3). Regarding the organotropism, results showed lowest Cs_b accumulations in the gills (~10 %), followed by the digestive gland (27 %, Fig. S1). This accumulation pattern may indicate a higher influence of the trophic pathway (Cs_p or biomagnification through the trophic chain) compared to the direct pathway (Cs_d). Nevertheless, it is also possible that the biological residence time of Cs in the gills is short, given the fact that Cs^+ can use the same intracellular transporter channels as K^+ and Ca^{2+} (e.g., Bryan, 1963; Harrison, 1972; Goudard et al., 1998). This would also explain why the highest content of Cs_b was found in the mantle (55 %, Fig. S1), the organ between the soft tissue of the organism and its shell. Thus, it is not possible to pinpoint the specific source explaining the overall trend and the anomalous events of Cs_b in the historical time series of wild oysters at La Fosse. One does not know (i) if the high Cs_d at the oceanic endmember was constant over 34 years, (ii) if there were periods of higher productivity, i.e., phytoplanktonic blooms, producing anomalies, or (iii) if there were specific watershed drainage events over time, associated to Cs_p estuarine releases from fresh SPM/MTZ expulsions, to specific water discharge regimes in the previous months to the sample collection, or to point anthropogenic discharges such as stable Cs_d releases from the Blayais NPP. In any case, longer time series for both Cs_b and Cs_d/Cs_p within the Gironde Estuary would help clarifying these observations and hypotheses. Overall, bioconcentration ratios of ~386–1220 L kg^{-1} were found for the wild oysters at La Fosse. These ratios are relatively low compared to other non-essential elements (e.g., ~10^5 for Ag and ~10^6 for Cd and Hg; Lanceleur et al., 2011b; Briant et al., 2017; Pougnet et al., 2021) but comparable to emerging metallic contaminants (e.g. ~ 10^3 for Pt; Abdou et al., 2018) reported for the same site.

5. Conclusion

This is the first study in the literature to show long-term Cs dynamics at the continent-ocean transition system, including particulate, dissolved and biological fractions. Our study suggests that in the freshwater

domain of the Lot-Garonne River watersheds, Cs dynamics is mainly influenced by the SPM drainage source (Massif Central vs Pyrenees vs local Riou Mort geology) and its hydrosedimentary conditions (e.g., dam retention influencing solid/liquid residence times, with potential temperature/biological seasonal influence). Once in the Gironde Estuary, Cs behaves nearly conservatively due to the main influence of the oceanic endmember. Departures from the conservative behavior are due to the age of the SPM (e.g., fresh vs old), modulated by the spatial-temporal variability of the salinity gradient (i.e., mainly cation exchange processes on the clay minerals). Natural sources related to water discharge seem to be the main driver of Cs bioaccumulation in wild oysters at the estuary mouth, though they have also shown to be sensitive bioindicators of anomalous event. In any case, the biological uptake of Cs is weaker (i.e., 3-6 orders of magnitude) than other non-essential elements.

This comprehensive work represents a mechanistic study that help understand the processes involved in the biogeochemical cycle of Cs. This information is of vital importance for designing post-accidental scenarios for hypothetical accidental releases of ^{137}Cs for the Gironde Estuary. A practical application of this kind of studies would be in decision making for the release of radioactive waters into coastal areas (i. e., measure followed in Japan for stored water from the Fukushima Daiichi NPP accident in 2023). The knowledge transfer from this study to other river basins and estuary systems could be applied via geochemical models, requiring Cs_d concentrations, SPM mineralogy and estuarine dynamics as input information, as long as the clay minerals are still the dominating phase.

CRediT authorship contribution statement

Teba Gil-Díaz: Writing – review & editing, Writing – original draft, Visualization, Validation, Supervision, Software, Methodology, Investigation, Funding acquisition, Formal analysis, Data curation, Conceptualization. **Frédérique Pougnet:** Project administration, Investigation. **Maëva Labassa:** Investigation. **Lionel Dutruch:** Investigation. **Melina Abdou:** Writing – review & editing, Investigation. **Alexandra Coynel:** Writing – review & editing, Resources, Project administration, Funding acquisition. **Frédérique Eyrolle:** Writing – review & editing, Funding acquisition. **Nicolas Briant:** Writing – review & editing, Investigation. **Joël Knoery:** Writing – review & editing, Resources, Funding acquisition. **Jörg Schäfer:** Supervision, Resources, Funding acquisition, Conceptualization.

Declaration of competing interest

The authors declare that they have no known competing financial interests or personal relationships that could have appeared to influence the work reported in this paper.

Data availability

Data will be made available on request.

Acknowledgements

current manager of the ROCCH. We are also grateful to the crew of the French Oceanographic R/V Thalia (sampling campaigns MGTS I doi 10.17600/14008300; MGTS II doi 10.17600/15009300; MGTS III doi 10.17600/15010600 and MGTS IV) and all TGM members that contributed to the sampling campaigns in the Lot-Garonne-Gironde fluvial-estuarine system.

Appendix A. Supplementary data

Supplementary data to this article can be found online at https://doi.org/10.1016/j.chemosphere.2024.142266.

References

Abdou, M., Tercier-Waeber, M.L., 2022. New insights into trace metal speciation and interaction with phytoplankton in estuarine coastal waters. Mar. Pollut. Bull. 181, 113845.

Abdou, M., Dutruch, L., Schäfer, J., Zaldibar, B., Medrano, R., Izagirre, U., Gil-Díaz, T., Bossy, C., Catrouillet, C., Hu, R., Coynel, A., Lerat, A., Cobelo-García, A., Blanc, G., Soto, M., 2018. Tracing platinum accumulation kinetics in oyster Crassostrea gigas, a sentinel species in coastal marine environments. Sci. Total Environ. 615, 652–663.

Allen, G.P., Salomon, J.C., Bassoullet, P., Du Penhoat, Y., De Grandpre, C., 1980. Effects of tides on mixing and suspended sediment transport in macrotidal estuaries. Sediment. Geol. 26, 69–90. https://doi.org/10.1016/0037-0738(80)90006-8.

Arnot, J.A., Gobas, F.A.P.C., 2006. A review of bioconcentration factor (BCF) and bioaccumulation factor (BAF) assessments for organic chemicals in aquatic organisms. Environ. Rev. 14, 257–297. https://doi.org/10.1139/A06-005.

Baeyens, B., Bradbury, M.H., 2004. Cation exchange capacity measurements on illite using the sodium and cesium isotope dilution technique: effects of the index cation, electrolyte concentration and competition: modeling. Clay Clay Miner. 52 (4), 421–431.

Bayülken, S., Başçetin, E., Güçlü, K., Apak, R., 2011. Investigation and modeling of cesium (I) adsorption by Turkish clays: bentonite, zeolite, sepiolite, and kaolinite. Environ. Prog. Sustain. Energy 30 (1), 70–80.

Bera, G., Yeager, K.M., Shim, M., Shiller, A.M., 2015. Anthropogenic stable cesium in water and sediment of a shallow estuary, St. Louis Bay, Mississippi. Estuar. Coast Shelf Sci. 157, 32–41.

Bradbury, M.H., Baeyens, B., 2000. A generalised sorption model for the concentration dependent uptake of caesium by argillaceous rocks. J. Contam. Hydrol. 42 (2–4), 141–163.

Briant, N., Chouvelon, T., Martinez, L., Brach-Papa, C., Chiffoleau, J.F., Savoye, N., Sonke, J., Knoery, J., 2017. Spatial and temporal distribution of mercury and methylmercury in bivalves from the French coastline. Mar. Pollut. Bull. 114 (2), 1096–1102.

Brouwer, E., Baeyens, B., Maes, A., Cremers, A., 1983. Cesium and rubidium ion equilibriums in illite clay. J. Phys. Chem. 87 (7), 1213–1219.

Bryan, G.W., 1963. The accumulation of radioactive caesium by marine invertebrates. J. Mar. Biol. Assoc. U. K. 43 (2), 519–539.

Bureau de Recherches Géologiques et Minières (BRGM), 1978. Carte des gîtes minéraux de la France à 1/500000e, feuille de LYON, Service Géologique National.

Bureau de Recherches Géologiques et Minières (BRGM), 1983. Carte des gîtes minéraux de la France à 1/500000e, feuille de BORDEAUX, Service Géologique National.

Bureau de Recherches Géologiques et Minières (BRGM, 2014. Carrières de France, exploitations actives. http://www.brgm.fr/actualite/brgm-sim-presentent-carte-carrieres-france. (Accessed 13 July 2015).

Castaing, P., Allen, G.P., 1981. Mechanisms controlling seaward escape of suspended sediment from the Gironde: a macrotidal estuary in France. Mar. Geol. 40, 101–118. https://doi.org/10.1016/0025-3227(81)90045-1.

Castaing, P., Jouanneau, J.M., 1979. Temps de résidence des eaux et des suspensions dans l'estuaire de la Gironde. Journal Recherche Océanographie IV, 41–52.

Comans, R.N., Hockley, D.E., 1992. Kinetics of cesium sorption on illite. Geochem. Cosmochim. Acta 56 (3), 1157–1164.

Coynel, A., Blanc, G., Marache, A., Schäfer, J., Dabrin, A., Maneux, E., Bossy, C., Masson, M., Lavaux, G., 2009. Assessment of metal contamination in a small mining- and smelting-affected watershed: high resolution monitoring coupled with spatial analysis by GIS. J. Environ. Monit. 11 (5), 962–976.

Daskalakis, K.D., O'Connor, T.P., Crecelius, E.A., 1997. Evaluation of digestion procedures for determining silver in mussels and oysters. Environ. Sci. Technol. 31, 2303–2306. https://doi.org/10.1021/ES9608959.

Delaval, A., Duffa, C., Radakovitch, O., 2020. A review on cesium desorption at the freshwater-seawater interface. J. Environ. Radioact. 218, 106255.

Desai, D.V., Sathi, S.K., Pillai, K.C., 1994. Influence of major cations of sea water on the desorption of 137Cs from marine sediments. J. Radioanal. Nucl. Chem. 187 (3), 197–205.

DIREN, 2023. National Hydrographic Databank. Ministère de l'Écologie, du Développement Durable et de l'Énergie. Available at: http://www.hydro.eaufrance.fr/. (Accessed 20 March 2023).

Doxaran, D., Froidefond, J.M., Castaing, P., Babin, M., 2009. Dynamics of the turbidity maximum zone in a macrotidal estuary (the Gironde, France): observations from field and MODIS satellite data. Estuar. Coast Shelf Sci. 81, 321–332. https://doi.org/10.1016/J.ECSS.2008.11.013.

Evrard, O., Laceby, J.P., Lepage, H., Onda, Y., Cerdan, O., Ayrault, S., 2015. Radiocesium transfer from hillslopes to the Pacific ocean after the Fukushima nuclear power plant accident: a review. J. Environ. Radioact. 148, 92–110.

Geological Survey, U.S., 2022. Cesium. By Cris Candice Tuck. U.S. Geological Survey Mineral Commodity Summaries. https://pubs.usgs.gov/periodicals/mcs2022/mcs2022-cesium.pdf. (Accessed 25 June 2023).

Gil-Díaz, T., Schäfer, J., Pougnet, F., Abdou, M., Dutruch, L., Eyrolle-Boyer, F., Coynel, A., Blanc, G., 2016. Distribution and geochemical behaviour of antimony in the Gironde estuary: a first qualitative approach to regional nuclear accident scenarios. Mar. Chem. 185, 65–73. https://doi.org/10.1016/J.MARCHEM.2016.02.002.

Gil-Díaz, T., Schäfer, J., Coynel, A., Bossy, C., Dutruch, L., Blanc, G., 2018. Antimony in the Lot–Garonne river system: a 14-year record of solid–liquid partitioning and fluxes. Environ. Chem. 15 (3), 121–136. https://doi.org/10.1071/EN17188.

Gil-Díaz, T., Schäfer, J., Dutruch, L., Bossy, C., Pougnet, F., Abdou, M., et al., 2019. Tellurium behaviour in a major European fluvial–estuarine system (Gironde, France): fluxes, solid/liquid partitioning and bioaccumulation in wild oysters. Environ. Chem. 16 (4), 229–242.

Gil-Díaz, T., Heberling, F., Keller, V., Fuss, M., Böttle, M., Eiche, E., Schäfer, J., 2020. Tin-113 and Selenium-75 radiotracer adsorption and desorption kinetics in contrasting estuarine salinity and turbidity conditions. J. Environ. Radioact. 213, 106133.

Goudard, F., Milcent, M.C., Durand, J.P., Germain, P., Paquet, F., Pieri, J., 1998. Subcellular and molecular Localisation of different radionuclides (cesium, Americum, Plutonium, and Technetium) in aquatic organisms. Radiat. Protect. Dosim. 75 (1–4), 117–124.

Gutierrez, M., Fuentes, H.R., 1996. A mechanistic modeling of montmorillonite contamination by cesium sorption. Appl. Clay Sci. 11 (1), 11–24.

Hanor, J.S., Chan, L.H., 1977. Non-conservative behavior of barium during mixing of Mississippi River and Gulf of Mexico waters. Earth Planet Sci. Lett. 37, 242–250.

Harrison, F.L., 1972. Accumulation and Loss of Cobalt and Cesium by the Marine Clam, *Mya arenaria*, under Laboratory and Field Conditions (No. UCRL-73744; CONF-720708-7). California Univ., Livermore. Lawrence Livermore Lab.

Iijima, K., Tomura, T., Shoji, Y., 2010. Reversibility and modeling of adsorption behavior of cesium ions on colloidal montmorillonite particles. Appl. Clay Sci. 49 (3), 262–268.

International Atomic Energy Agency (IAEA, 2004. Sediment Distribution Coefficients and Concentration Factors for Biota in the Marine Environment. International Atomic Energy Agency, Vienna, Austria.

Jouanneau, J.M., Latouche, C., 1981. The Gironde Estuary. Schweizerbart Science Publishers, Stuttgart, Germany.

Kabata-Pendias, A., 2011. Trace Elements in Soils and Plants. CRC Press, Boca Raton, FL.

Khan, A.N., Bagla, H.K., 2022. Batch adsorption and desorption investigations of Cs (I) and Sr (II) from simulated reactor waste by humic acid. Journal of Trace Elements and Minerals 1, 100005.

Krachler, M., Shotyk, W., 2004. Natural and anthropogenic enrichments of molybdenum, thorium and uranium in a complete peat bog profile, Jura Mountains, Switzerland. J. Environ. Monit. 6, 418–426.

Laissaoui, A., Abril, J.M., Periáñez, R., León, M.G., Montaño, E.G., 1998. Kinetic transfer coefficients for radionuclides in estuarine waters: reference values from 133Ba and effects of salinity and suspended load concentration. J. Radioanal. Nucl. Chem. 237, 55–62.

Lanceleur, L., Schäfer, J., Bossy, C., Coynel, A., Larrose, A., Masson, M., Blanc, G., 2011a. Silver fluxes to the Gironde Estuary–Eleven years (1999–2009) of monitoring at the watershed scale. Appl. Geochem. 26, 797–808. https://doi.org/10.1016/J.APGEOCHEM.2011.02.001.

Lanceleur, L., Schäfer, J., Chiffoleau, J.F., Blanc, G., Auger, D., Renault, S., Baudrimont, M., Audry, S., 2011b. Long-term records of cadmium and silver contamination in sediments and oysters from the Gironde fluvial– estuarine continuum – Evidence of changing silver sources. Chemosphere 85, 1299–1305. https://doi.org/10.1016/J.CHEMOSPHERE.2011.07.036.

Lapaquellerie, Y., Maillet, N., Jouanneau, J.-M., Coakley, J.P., Latouche, C., 1996. Flux de matières en suspension et de cadmium dans le Lot. Hydroécol. Appliquée 8, 173–191. https://doi.org/10.1051/HYDRO:1996008.

Larrose, A., Coynel, A., Schäfer, J., Blanc, G., Massé, L., Maneux, E., 2010. Assessing the current state of the Gironde Estuary by mapping priority contaminant distribution and risk potential in surface sediment. Appl. Geochem. 25, 1912–1923.

Lekhi, P., Cassis, D., Pearce, C.M., Ebell, N., Maldonado, M.T., Orians, K.J., 2008. Role of dissolved and particulate cadmium in the accumulation of cadmium in cultured oysters (*Crassostrea gigas*). Sci. Total Environ. 393, 309–325. https://doi.org/10.1016/J.SCITOTENV.2007.12.004.

Lerat-Hardy, A., Coynel, A., Dutruch, L., Pereto, C., Bossy, C., Gil-Díaz, T., Capdeville, M. J., Blanc, G., Schäfer, J., 2019. Rare Earth Element fluxes over 15 years into a major European Estuary (Garonne-Gironde, SW France): Hospital effluents as a chance of increasing gadolinium anomalies. Sci. Total Environ. 656, 409–420. https://doi.org/10.1016/J.SCITOTENV.2018.11.343.

Loring, D.H., Rantala, R.T.T., 1992. Manual for the geochemical analyses of marine sediments and suspended particulate matter. Earth Sci. Rev. 32 (4), 235–283.

Masson, M., 2007. Sources et transferts métalliques dans le bassin versant de la Gironde: Réactivité et mécanismes géochimiques dans l'estuaire fluvial de la Gironde (doctoral dissertation, Bordeaux 1).

Masson, M., Schäfer, J., Blanc, G., Anschutz, P., 2007. Seasonal variations and annual fluxes of arsenic in the Garonne, Dordogne and Isle rivers, France. Sci. Total Environ. 373, 196–207. https://doi.org/10.1016/J.SCITOTENV.2006.10.039.

McKinley, I.G., Alexander, W.R., 1992. Constraints on the applicability of 'in-situ distribution coefficient' values. J. Environ. Radioact. 15 (1), 19–34.

Metwally, E., Abdel Rahman, R.O., Ayoub, R.R., 2007. Modeling batch kinetics of cesium, cobalt and strontium ions adsorption from aqueous solutions using hydrous titanium oxide. Radiochim. Acta 95 (7), 409–416.

Meybeck, M., Ragu, A., 1995. River Discharges to the Oceans: an Assessment of Suspended Solids, Major Ions, and Nutrients. ' (UNEP, Nairobi.

Meybeck, M., Pasco, A., Ragu, A., 1994. Etablissement des flux polluants dans les rivières: pourquoi, comment et à quel prix. 4eme Rencontres de l'Agence Régionale pour l'environnement. In: Provence-Alpes-Côte d'Azur. Colloque scientifique sur les charges polluantes véhiculées par les fleuves et les rivières en Méditerranée.

Missana, T., Alonso, U., García-Gutiérrez, M., 2009. Experimental study and modelling of selenite sorption onto illite and smectite clays. J. Colloid Interface Sci. 334 (2), 132–138.

Missana, T., Benedicto, A., García-Gutiérrez, M., Alonso, U., 2014. Modeling cesium retention onto Na-, K-and Ca-smectite: effects of ionic strength, exchange and competing cations on the determination of selectivity coefficients. Geochem. Cosmochim. Acta 128, 266–277.

Mukai, H., Tamura, K., Kikuchi, R., Takahashi, Y., Yaita, T., Kogure, T., 2018. Cesium desorption behavior of weathered biotite in Fukushima considering the actual radioactive contamination level of soils. J. Environ. Radioact. 190–191, 81–88. https://doi.org/10.1016/j.jenvrad.2018.05.006.

Nakao, A., Ogasawara, S., Sano, O., Ito, T., Yanai, J., 2014. Radiocesium sorption in relation to clay mineralogy of paddy soils in Fukushima, Japan. Sci. Total Environ. 469, 523–529.

Nanba, K., Moritaka, S., Igarashi, Y., 2022. Chapter 8. Dynamics of radiocesium in urban river in Fukushima city. In: Nanba, K., Konoplev, A., Wada, T. (Eds.), Behavior of Radionuclides in the Environment III: Fukushima. Springer Nature.

Naulier, M., Eyrolle-Boyer, F., Boyer, P., Métivier, J., Onda, Y., 2017. Particulate organic matter in rivers of Fukushima : an unexpected carrier phase for radiocesiums. Sci. Total Environ. 579, 1560–1571. https://doi.org/10.1016/j.scitotenv.2016.11.165.

Nie, Z., Finck, N., Heberling, F., Pruessmann, T., Liu, C., Lützenkirchen, J., 2017. Adsorption of selenium and strontium on goethite: EXAFS study and surface complexation modeling of the ternary systems. Environ. Sci. Technol. 51 (7), 3751–3758.

Okumura, M., Kerisit, S., Bourg, I.C., Lammers, L.N., Ikeda, T., Sassi, M., Machida, M., 2018. Radiocesium interaction with clay minerals: theory and simulation advances Post–Fukushima. J. Environ. Radioact. 189, 135–145. https://doi.org/10.1016/j.jenvrad.2018.03.011.

Olsen, C.R., Simpson, H.J., Trier, R.M., 1981. Plutonium, radiocesium and radiocobalt in sediments of the Hudson River estuary. Earth Planet Sci. Lett. 55, 292–377.

Onishi, Y., Serne, R., Arnold, E., Cowen, C., Thompson, J., 1981. Critical review: radionuclide transport, sediment transport, and water Quality Mathematical modeling; and radionuclide adsorption/desorption mechanisms. Technical report Battelle Pacific Northwest Labs, Richland, WA (United States).

Onodera, M., Kirishima, A., Nagao, S., Takamiya, K., Ohtsuki, T., Akiyama, D., Sato, N., 2017. Desorption of radioactive cesium by seawater from the suspended particles in river water. Chemosphere 185, 806–815. https://doi.org/10.1016/j.chemosphere.2017.07.078.

OSPAR, 2018. Available at: http://www.ospar.org. (Accessed 3 August 2018).

Parkhurst, D.L., Appelo, C.A.J., 1999. User's guide to PHREEQC (Version 2): a computer program for speciation, batch-reaction, one-dimensional transport, and inverse geochemical calculations. Water-resources investigations report 99 (4259), 312.

Periáñez, R.R., 2005. Modelling the transport of suspended particulate matter by the Rhone River plume (France). Implications for pollutant dispersion. Environ. Pollut. 133 (2), 351–364.

Periáñez, R., Elliott, A.J., 2002. A particle-tracking method for simulating the dispersion of non-conservative radionuclides in coastal waters. J. Environ. Radioact. 58 (1), 13–33.

Poinssot, C., Baeyens, B., Bradbury, M.H., 1999. Experimental and modelling studies of caesium sorption on illite. Geochem. Cosmochim. Acta 63 (19–20), 3217–3227.

Pougnet, F., Blanc, G., Mulamba-Guilhemat, E., Coynel, A., Gil-Díaz, T., Bossy, C., et al., 2021. Nouveau modèle analytique pour une meilleure estimation des flux nets annuels en métaux dissous. Cas du cadmium dans l'estuaire de la Gironde. Hydroécol. Appliquée 21, 47–69.

Pougnet, F., Gil-Díaz, T., Blanc, G., Coynel, A., Bossy, C., Schäfer, J., 2022. Historical mass balance of cadmium decontamination trends in a major European continent-ocean transition system: case study of the Gironde Estuary. Mar. Environ. Res. 176, 105594.

Rankin, D.W.H., 2009. CRC handbook of chemistry and physics, 89th edition, edited by David R. Lide. Crystallogr. Rev. 15 (3), 223–224. https://doi.org/10.1080/08893119902764125.

Reimann, C., de Caritat, P.D., 2000. Intrinsic flaws of element enrichment factors (EFs) in environmental geochemistry. Environ. Sci. Technol. 34 (24), 5084–5091.

Saito, K., Tanihata, I., Fujiwara, M., Saito, T., Shimoura, S., Otsuka, T., Onda, Y., Hoshi, M., Ikeuchi, Y., Takahashi, F., Kinouchi, N., Saegusa, J., Seki, A., Takemiya, H., Shibata, T., 2015. Detailed deposition density maps constructed by large-scale soil sampling for gamma-ray emitting radioactive nuclides from the Fukushima Dai-ichi Nuclear Power Plant accident. J. Environ. Radioact. 139, 308–319.

Salminen, R., Batista, M.J., Bidovec, M., Demetriades, A., De Vivo, B., De Vos, W., Duris, M., Gilucis, A., Gregorauskiene, V., Halamic, J., Heitzmann, P., Lima, A.,

Jordan, G., Klaver, G., Klein, P., Lis, J., Locutura, J., Marsina, K., Mazreku, A., O'Connor, P.J., Olsson, S.A., Ottesen, R.T., Petersell, V., Plant, J.A., Reeder, S., Salpeteur, I., Sandström, H., Siewers, U., Steenfelt, A., Tarvainen, T., 2005. Geochemical Atlas of Europe. Part 1 – Background Information, Methodology and Maps. Geological Survey of Finland (Espoo, Finland).

Salomon, J.N., 2002. L'inondation dans la basse vallée de la Garonne et l'estuaire de la Gironde lors de la. Géomorphol. Relief, Process. Environ. 8, 127–134. https://doi.org/10.3406/MORFO.2002.1134.

Sanial, V., Buesseler, K.O., Charette, M.A., Nagao, S., 2017. Unexpected source of Fukushima-derived radiocesium to the coastal ocean of Japan. Proc. Natl. Acad. Sci. USA 114 (42), 11092–11096.

Schäfer, J., Blanc, G., Lapaquellerie, Y., Maillet, N., Maneux, E., Etcheber, H., 2002. Ten-year-observation of the Gironde fluvial system: fluxes of suspended matter, particulate organic carbon and cadmium. Mar. Chem. 79, 229–242. https://doi.org/10.1016/S0304-4203(02)00066-X.

Sheha, R.R., Metwally, E., 2007. Equilibrium isotherm modeling of cesium adsorption onto magnetic materials. J. Hazard Mater. 143 (1–2), 354–361.

Shiller, A.M., 1997. Dissolved trace elements in the Mississippi River: seasonal, interannual, and decadal variability. Geochem. Cosmochim. Acta 61, 4321–4330. https://doi.org/10.1016/S0016-7037(97)00245-7.

Shiller, A.M., Mao, L., 1999. Dissolved vanadium on the Louisiana Shelf: effect of oxygen depletion. Continent. Shelf Res. 19, 1007–1020. https://doi.org/10.1016/S0278-4343(99)00005-9.

Shiller, A.M., Mao, L., 2000. Dissolved vanadium in rivers: effects of silicate weathering. Chem. Geol. 165, 13–22. https://doi.org/10.1016/S0009-2541(99)00160-6.

Shim, M.J., Swarzenski, P.W., Shiller, A.M., 2012. Dissolved and colloidal trace elements in the Mississippi River delta outflow after Hurricanes Katrina and Rita. Continent. Shelf Res. 42, 1–9.

Sottolichio, A., Castaing, P., 1999. A synthesis on seasonal dynamics of highly-concentrated structures in the Gironde estuary. Comptes Rendus de l'Acaéemie des Sciences Series IIA: Earth and Planetary Science 329, 795–800.

Sposito, G., Skipper, N.T., Sutton, R., Park, S.H., Soper, A.K., Greathouse, J.A., 1999. Surface geochemistry of the clay minerals. Proc. Natl. Acad. Sci. U.S.A. 96 (7), 3358–3364. https://doi.org/10.1073/pnas.96.7.3358.

Sung, W., 1995. Some observations on surface partitioning of Cd, Cu and Zn in estuaries. Environ. Sci. Technol. 29, 1303–1312. https://doi.org/10.1021/ES00005A024.

Tagami, K., Uchida, S., 2013. Sediment-seawater distribution coefficient for radionuclides and estimation of radionuclide desorption ratio from soil in seawater (Abstract in English). Bunseki Kagaku 62, 527e533.

Takata, H., Aono, T., Zheng, J., Tagami, K., Shirasaka, J., Uchida, S., 2013. A sensitive and simple analytical method for the determination of stable Cs in estuarine and coastal waters. Anal. Methods 5 (10), 2558–2564.

Tomczak, W., Boyer, P., Krimissa, M., Radakovitch, O., 2019. Kd distributions in freshwater systems as a function of material type, mass-volume ratio, dissolved organic carbon and pH. Appl. Geochem. 105, 68–77.

U.S. Environmental Protection Agency (USEPA), 2000. Methods for Measuring the Toxicity and Bioaccumulation of Sediment-Associated Contaminants with Freshwater Invertebrates, second ed. EPA 600/R-99/064.

U.S. Environmental Protection Agency (USEPA), 2007. Determination of Trace Metals by SW-846. Method 6020A. Inductively Coupled Plasmamass Spectrometry. EPA, Washington, D.C.

Volpe, A.M., Bandong, B.B., Esser, B.K., Bianchini, G.M., 2002. Radiocesium in north San Francisco bay and Baja California coastal surface waters. J. Environ. Radioact. 60, 365–380.

Wakiyama, Y., Konoplev, A., Thoa, N., Niida, T., Tsukada, H., Takase, T., Nanba, K., Golosov, V., Zheleznyak, M., 2022. Chapter 9. Temporal variations in particulate and dissolved 137Cs activity concentrations in the Abukuma river during two high-flow events in 2018. In: Nanba, K., Konoplev, A., Wada, T. (Eds.), Behavior of Radionuclides in the Environment III: Fukushima. Springer Nature.

Wauters, J., Vidal, M., Elsen, A., Cremers, A., 1996. Prediction of solid/liquid distribution coefficients of radiocaesium in soils and sediments. Part two: a new procedure for solid phase speciation of radiocaesium. Appl. Geochem. 11 (4), 595–599. https://doi.org/10.1016/0883-2927(96)00028-5.

Webb, B.W., Phillips, J.M., Walling, D.E., Littlewood, I.G., Watts, C., Leeks, G.J.L., 1997. Load estimation methodologies for British river and their relevance to the LOIS RACS (R) program. Sci. Total Environ. 194–195, 379–389. https://doi.org/10.1016/S0048-9697(96)05377-6.

Zachara, J.M., Smith, S.C., Liu, C., McKinley, J.P., Serne, R.J., Gassman, P.L., 2002. Sorption of Cs+ to micaceous subsurface sediments from the Hanford site, USA. Geochem. Cosmochim. Acta 66 (2), 193–211. https://doi.org/10.1016/S0016-7037(01)00759-1.

Zaunbrecher, L.K., Cygan, R.T., Elliott, W.C., 2015. Molecular models of cesium and rubidium adsorption on weathered micaceous minerals. J. Phys. Chem. A 119 (22), 5691–5700.

Zheleznyak, M., Kivva, S., Pylypenko, O., Sorokin, M., 2022. Chapter 11. Modeling of behaviour of Fukushima-derived radionuclides in freshwater systems. In: Nanba, K., Konoplev, A., Wada, T. (Eds.), Behavior of Radionuclides in the Environment III: Fukushima. Springer Nature.